Aus dem Institut für Molekulare Medizin I
der Heinrich-Heine-Universität Düsseldorf
Direktor: Univ.-Prof. Dr. Sebastian Wesselborg

Hsp90 inhibitors work synergistically with mTOR inhibition to kill bladder cancer cells

Dissertation

zur Erlangung des Grades eines Doktors der Medizin
der Medizinischen Fakultät der Heinrich-Heine-Universität Düsseldorf

vorgelegt von

Yadong Sun

2021

Als Inauguraldissertation gedruckt mit der Genehmigung der

Medizinischen Fakultät der Heinrich-Heine-Universität Düsseldorf

gez.:

Dekan/in: Prof. Dr. med. Nikolaj Klöcker

Erstgutachter/in: Prof. Dr. rer. nat. Björn Stork

Zweitgutacher/in: Prof. Dr. med. Günter Niegisch

千里之行，始于足下。

The journey of a thousand miles starts with a single step.

Publications

The following papers have been published during my MD but are not part of this thesis:

Sun Y, Berleth N, Wu W, Schlütermann D, Deitersen J, Stuhldreier F, Berning L, Friedrich A, Akgün S, Mendiburo M, Wesselborg S, Conrad M, Berndt C and Stork B. (2021) Fin56-induced ferroptosis is supported by autophagy mediated GPX4 degradation and functions synergistically with mTOR inhibition to kill bladder cancer cells. **Cell Death & Disease**. 12(11):1028.

Wu W, Wang X, **Sun Y**, Berleth N, Deitersen J, Schlütermann D, Stuhldreier F, Wallot-Hieke N, Mendiburo M, Cox J, Peter C, Gergmann A and Stork B. (2021) TNF-induced necroptosis initiates early autophagy events via RIPK3-dependent AMPK activation, but inhibits late autophagy. **Autophagy**. 28;1-18

Berning L, Schlütermann D, Friedrich A, Berleth N, **Sun Y**, Wu W, Mendiburo M, Deitersen J, Brass H, Skowron M, Hoffmann M, Niegisch G, Pietruszka J and Stork B. (2021) Prodigiosin Sensitizes Sensitive and Resistant Urothelial Carcinoma Cells to Cisplatin Treatment. **Molecules**. 26(5):1294

Schlütermann D, Berleth N, Deitersen J, Wallot-Hieke N, Friesen O, Wu W, Stuhldreier F, **Sun Y**, Berning L, Friedrich A, Mendiburo M, Peter C, Wiek C, Hanenberg H, Stefanski A, Stuehler K and Stork B. (2021) FIP200 controls the TBK1 activation threshold at SQSTM1/p62-positive condensates. **Scientific Reports**. 11(1):13863

Deitersen J, Berning L, Stuhldreier F, Ceccacci S, Schlütermann D, Friedrich A, Wu W, **Sun Y**, Böhler P, Berleth N, Mendiburo M, Seggewiß S, Anand R, Reichert A, Monti M, Chaidir C and Stork B. (2021) High-throughput screening for natural compound-based autophagy modulators reveals novel chemotherapeutic mode of action for arzanol. **Cell Death & Disease**. 12(6):560

Zusammenfassung

Harnblasenkrebs ist der am dritthäufigsten diagnostizierte Krebs in Europa. Aufgrund der hohen Induktionsrate und der ineffizienten Behandlungsmethoden stellt Blasenkrebs in der EU eine große wirtschaftliche und gesundheitliche Belastung dar. Eine Chemotherapie auf Cisplatin-Basis ist seit den späten 1980er Jahren die Erstlinienbehandlung für fortgeschrittenen Blasenkrebs. Trotz aggressiver Chemotherapie ist die relative 5-Jahres-Überlebensrate von Blasenkrebspatienten in den letzten drei Jahrzehnten praktisch unverändert geblieben. Die hohe Inzidenz von Chemoresistenz und die Zytotoxizität von Cisplatin wie Neurotoxizität, Nephrotoxizität und Ototoxizität sind die wichtigsten Einschränkungen für den klinischen Einsatz von Cisplatin. Es besteht ein dringender Bedarf, Methoden zu finden, um die Nebenwirkungen von Cisplatin zu reduzieren und Cisplatin-resistente Krebszellen für die Behandlung mit Cisplatin zu resensibilisieren.

mTOR-Inhibitoren wurden ausgiebig als Anti-Tumor-Reagenzien gegen verschiedene Krebsarten untersucht, darunter Brustkrebs, Lungenkrebs, Magenkarzinom, Prostatakrebs und Blasenkrebs. Einige von ihnen befinden sich in verschiedenen Phasen klinischer Studien und haben vielversprechende Effekte bei der Hemmung von Proliferation und Wachstum von Krebszellen gezeigt. Allerdings wird die Wirkung von mTOR-Inhibitoren, die als Monotherapie eingesetzt werden, manchmal durch verschiedene Resistenzmechanismen gedämpft. Ein sehr wichtiger Aspekt ist dabei die Unterdrückung negativer Rückkopplungsschleifen, durch die es zu einer mehrfachen Überaktivierung alternativer proliferativer Signalwege kommt. Viele Hub-Proteine dieser Signalwege sind Hsp90-Client-Proteine, wie MEK, IRS2, HER3 und AKT. Daher wird erwartet, dass die Kombination von mTOR-Inhibitoren und Hsp90-Inhibitoren die therapeutische Wirkung verbessert.

In dieser Arbeit wurden zwei Hsp90-Inhibitoren (die auf das C-terminale oder N-terminale Ende von Hsp90 abzielen) verwendet. Ihre Effekte wurden mittels Immunoblot-Analysen in den Blasenkrebs-Zelllinien J82, 253J, T24, RT-112 und den entsprechenden Cisplatin-resistenten Zellen evaluiert. Der alamarBlue Assay wurde verwendet, um die Zellviabilität nach der Behandlung mit mTOR-Inhibitoren, HSP90-Inhibitoren und deren Kombinationen in Cisplatin-sensitiven und -resistenten BCs zu analysieren. Unabhängig davon, ob sie allein oder in Kombination verwendet wurden, zeigten alle in dieser Arbeit verwendeten Inhibitoren eine

hohe Zytotoxizität für Blasenkrebszellen. Bemerkenswert ist, dass der C-terminale Hsp90-Inhibitor eine synergistische Interaktion mit dem mTOR-Inhibitor sowohl bei Cisplatin-sensitiven als auch -resistenten Zellen zeigte, während der N-terminale Hsp90-Inhibitor nur bei Cisplatin-sensitiven Zellen synergistisch mit dem mTOR-Inhibitor wirkte. Darüber hinaus induzierte der C-terminale Hsp90-Inhibitor, aber nicht der N-terminale Inhibitor, eine nicht-kanonische LC3-Lipidierung in den getesteten Blasenkrebs-Zelllinien. Die Funktion der induzierten LC3-Lipidierung und ob sie an der synergistischen Interaktion mit mTOR-Inhibitoren beteiligt ist, muss weiter untersucht werden.

Zusammenfassend lässt sich sagen, dass die Kombination von Hsp90-Inhibitoren und mTOR-Inhibitoren eine vielversprechende Chemotherapie-Methode gegen Blasenkrebs sein könnte, insbesondere für C-terminale Hsp90-Inhibitoren, die verwendet werden können, um Cisplatin-resistente Zellen für Cisplatin zu resensibilisieren.

Summary

Urinary bladder cancer (BC) is the third most commonly diagnosed cancer in Europe. Due to the high induction rate and inefficient treatment methods, bladder cancer has caused a heavy economic and health burden in the EU. Cisplatin-based chemotherapy has been the first-line treatment for advanced BC since the late 1980s. Despite aggressive chemotherapy treatment, the 5-year relative survival rates of BC patients have been virtually unchanged over the past 3 decades. The high incidence of chemoresistance and cytotoxicity of cisplatin, such as neurotoxicity, nephrotoxicity and ototoxicity are the main limitations of clinical use of cisplatin. There is an urgent need to find methods to reduce the side effects of cisplatin and to resensitize cisplatin-resistant cancer cells to cisplatin treatment.

mTOR inhibitors have been extensively studied as anti-tumor reagents against a variety of cancers, including breast cancer, lung cancer, gastric carcinoma, prostate cancer, and bladder cancer. Some of them are involved in multiple phases of clinical trials and have demonstrated promising effects in inhibiting the proliferation and growth of cancer cells. However, the role of mTOR inhibitors as monotherapy is sometimes dampened by multiple resistance mechanisms. Among them, one of the most important is the suppression of negative feedback loop, which induces multiple overactivation of alternate proliferative signaling pathways. Many hub proteins of these pathways are Hsp90 client proteins, such as MEK, IRS2, HER3 and AKT. Therefore, the combination of mTOR inhibitors and Hsp90 inhibitors is expected to improve the therapeutic effects.

Two Hsp90 inhibitors (targeting the C terminus or N terminus of Hsp90) were used in this thesis. Their effects are evaluated using immunoblotting in the BC cell lines J82, 253J, T24, RT-112, and corresponding cisplatin-resistant cells. The alamarBlue assay was used to analyze the cell viability upon the treatment with mTOR inhibitors, HSP90 inhibitors, and their combinations in cisplatin-sensitive and drug-resistant BCs. Whether used alone or in combination, all inhibitors used in this thesis showed high cytotoxicity to bladder cancer cells. Noteworthy, the C-terminal Hsp90 inhibitor exhibited a synergistic interaction with mTOR inhibitor in both cisplatin-sensitive and -resistant cells, whereas the N-terminal Hsp90 inhibitor only worked synergistically with mTOR inhibitor in cisplatin-sensitive cells. In addition, the C-terminal

Hsp90 inhibitor, but not N-terminal inhibitor, induced non-canonical LC3 lipidation in tested bladder cancer cell lines. The function of induced LC3 lipidation and whether it participates in the synergistic interaction with mTOR inhibitors needs further investigation.

In conclusion, the combination of Hsp90 inhibitors and mTOR inhibitors may be a promising chemotherapy method against bladder cancer.

List of abbreviations

AKT	protein kinase B (PKB, also known as AKT)
Amp	ampicillin (or ampicillin resistance gene)
AMPK	adenosine 5'-monophosphate-activated protein kinase
ATG	autophagy related (gene or protein)
ATP	adenosine triphosphate
ATPase	adenosine triphosphatase
Baf.A1	bafilomycin A_1
BC	bladder cancer
BCL-2	B cell lymphoma 2
BECN1	coiled-coil myosin-like BCL2-interacting protein
BSA	bovine serum albumin
CDC37	cell division cycle 37
CI	combination index
c-RAF	proto-oncogene serine/threonine-protein kinase
CRs	cisplatin resistant cells
DNA	deoxyribonucleic acid
dH_2O	deionized H2O
DMEM	Dulbecco's modified Eagle's medium
DMSO	dimethyl sulfoxide
DPBS	Dulbecco's phosphate-buffered saline
E. coli	Escherichia coli
EBSS	Earle's buffered salt solution
EDTA	Ethylenediaminetetraacetic acid
ER	endoplasmic reticulum
EtOH	ethanol
FCS	fetal calf serum
FIP200	focal adhesion family interacting protein of 200 kDa
GAPDH	glyceraldehyde-3-phosphate dehydrogenase
GFP	green fluorescent protein

HEK	human embryonic kidney
HSC70	heat shock-cognate protein of 70 kDa
HSR	heat shock response
Hsp90	heat shock protein 90 kDa
IB	immunoblot
IC50	half maximal inhibitory concentration
IF	immunofluorescence
IM	isolation membrane
IP	immunopurification
LB	lysis buffer
LC3	microtubule-associated proteins 1A/1B light chain 3
MAP1LC3B	microtubule-associated proteins 1A/1B light chain 3B
MEF	mouse embryonic fibroblast
MeOH	methanol
MIBC	muscle-invasive bladder cancer
mTOR	mechanistic target of rapamycin
MW	molecular weight
NH_4Cl	Ammonium chloride
NMIBC	non-muscle-invasive bladder cancer
P	phospho (as prefix)
PAGE	polyacrylamide gel electrophoresis
PBS	Phosphate-buffered saline
PE	phosphatidylethanolamine
PFA	paraformaldehyde
Plat-E	platinum E
P62	sequestosome 1 (SQSTM1, also known as P62)
PtdIns	phospatidylinositol
PVDF	polyvinylidenfluorid
Rapamycin	marcrolide from Streptomyces hygroscopicus
Raptor	regulatory associated protein of mTOR
RIPK1	receptor-interacting serine/threonine-protein kinase 1

RPMI	Roswell Park Memorial Institute
RT	room temperature
SD	standard deviation
SDS-PAGE	sodium dodecyl sulfate–polyacrylamide gel electrophoresis
SEM	standard error of the mean
siRNA	small interfering RNA
SQSTM1	Sequestosome-1
Tris	Tris-(hydroxymethyl)-aminomethane
Triton X-100	4-(2',2',4',4'-tetramethylbutyl) phenyldecaethylene-glycolether
TSC1/2	tuberous sclerosis 1/2
Tween 20	polyoxyethylene (20) sorbitan monolaurate
UBC	urinary bladder cancer
ULK	UNC-51-like kinase
UNC-51	uncoordinated movement-51
w/v	weight per volume
WIPI2	WD repeat domain phosphoinositide interacting 2
WT	wild-type
17-AAG	17-N-allylamino-17-emethoxygeldanamycin

Prefixes

p (pico) 10^{-12}

n (nano) 10^{-9}

μ (micro) 10^{-6}

m (milli) 10^{-3}

c (centi) 10^{-2}

k (kilo) 10^{3}

M (mega) 10^{6}

Units

s	second	Da	Dalton
min	minute	V	volt
h	hour	A	ampere
g	gram or local gravity	pH	$-\log10(a_{H+})$
L	liter	℃	degree Celsius
M	molar (mole/L)	rpm	rounds per minute
U	enzyme unit	Pa	pascal
psi	pounds per square inch		

Amino acids

	single-letter	three-letter code
Alanine	A	Ala
Cysteine	C	Cys
Aspartic acid	D	Asp
Glutamic acid	E	Glu
Phenylalanine	F	Phe
Glycine	G	Gly
Histidine	H	His
Isoleucine	I	Ile
Lysine	K	Lys
Leucine	L	Leu
Methionine	M	Met
Asparagine	N	Asn
Proline	P	Pro
Glutamine	Q	Gln
Arginine	R	Arg
Serine	S	Ser
Threonine	T	Thr
Valine	V	Val
Tryptophan	W	Trp
Tyrosine	Y	Tyr

Table of contents

1.Introduction

1.1 Bladder cancer

1.1.1 Epidemiology of bladder cancer

Bladder cancer (BC), also known as urinary bladder cancer, is the third most commonly diagnosed cancer in Europe, with an estimated 197,100 newly diagnosed cases and 65,000 of deaths in 2018 [1]. According to GLOBOCAN data, the number of diagnoses of BC accounts for about 3% of all new cancer diagnoses. Due to rising smoking rates and an aging population, the incidences of BC are relatively high and steadily rising in European countries, and is expected to increase even further. Among European nations, Greece has the highest incidence rates of BC, where an estimated 21.2/100,000 people develop the disease every year (regardless of gender and age). In Germany, the incidence and mortality of bladder cancer are moderate. It is estimated that 15.7/100,000 and 2.9/100,000 people suffer from the disease and die each year (Figure 1.1.1). Although immunotherapy, earlier diagnoses and robotic surgical techniques have improved survival rates, bladder cancer is still an important and increasing factor in the burden of cancer worldwide, especially in developed countries.

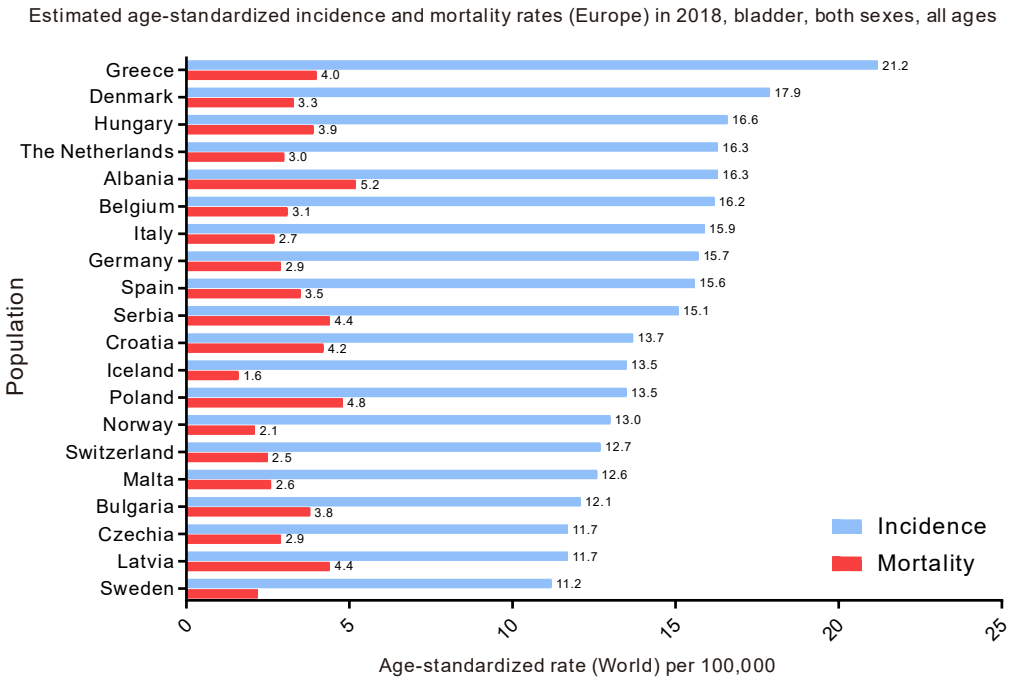

Figure 1.1.1: Estimated age-standardized incidence and mortality rates (Europe) in 2018, bladder cancer, all sexes, all ages. Data obtained from GLOBOCAN 2018, and only showed top 20 countries**.**

1.1.2 Pathology and treatment of bladder cancer

BC can be classified into two subtypes, namely non-muscle-invasive bladder cancer (NMIBC) and muscle-invasive bladder cancer (MIBC). Approximately 20% of newly diagnosed patients with muscle invasion, nodal or metastatic disease [2, 3], associated with moderate treatment response and survival rates [4–6]. Among the NMIBC patients, 10%–15% suffer disease progression, and 50%–70% have disease recurrence even under proper treatment [7]. With the help of numerous gene expression and next-generation sequencing studies, scientists and urologists have gradually realized that NMIBCs or MIBCs themselves are biologically heterogeneous, and clinical outcomes and responses to chemotherapy are diverse. Accordingly, a molecular taxonomy for bladder cancer was founded [8–10]. According to a European multicenter prospective study of NMIBC (UROMOL), the NMIBCs can be classified into three classes [11]. Correspondingly, MIBC can be divided into six subgroups [12]. The clinical stages and molecular subclasses of BC are represented in figure 1.1.2.

Cisplatin-based chemotherapy has been the first line treatment for advanced BC since the late 1980's [13]. Cisplatin is mainly used as neoadjuvant (before surgery) or adjuvant (after surgery) therapy regents. Cisplatin-containing combination chemotherapy is recommended used as neoadjuvant for MIBC, since it improves overall survival (OS) (8% at five years) [14]. Despite aggressive chemotherapy treatment, the 5-year relative survival percent for BC has been virtually unchanged over the past 3 decades [15]. The high incidence of chemoresistance and cytotoxicity of cisplatin such as neurotoxicity, nephrotoxicity and ototoxicity are the main limitation for the clinical usage of cisplatin [16, 17]. Aside from reducing side effects of cisplatin, circumventing cisplatin resistance is the major objective for BC chemotherapy.

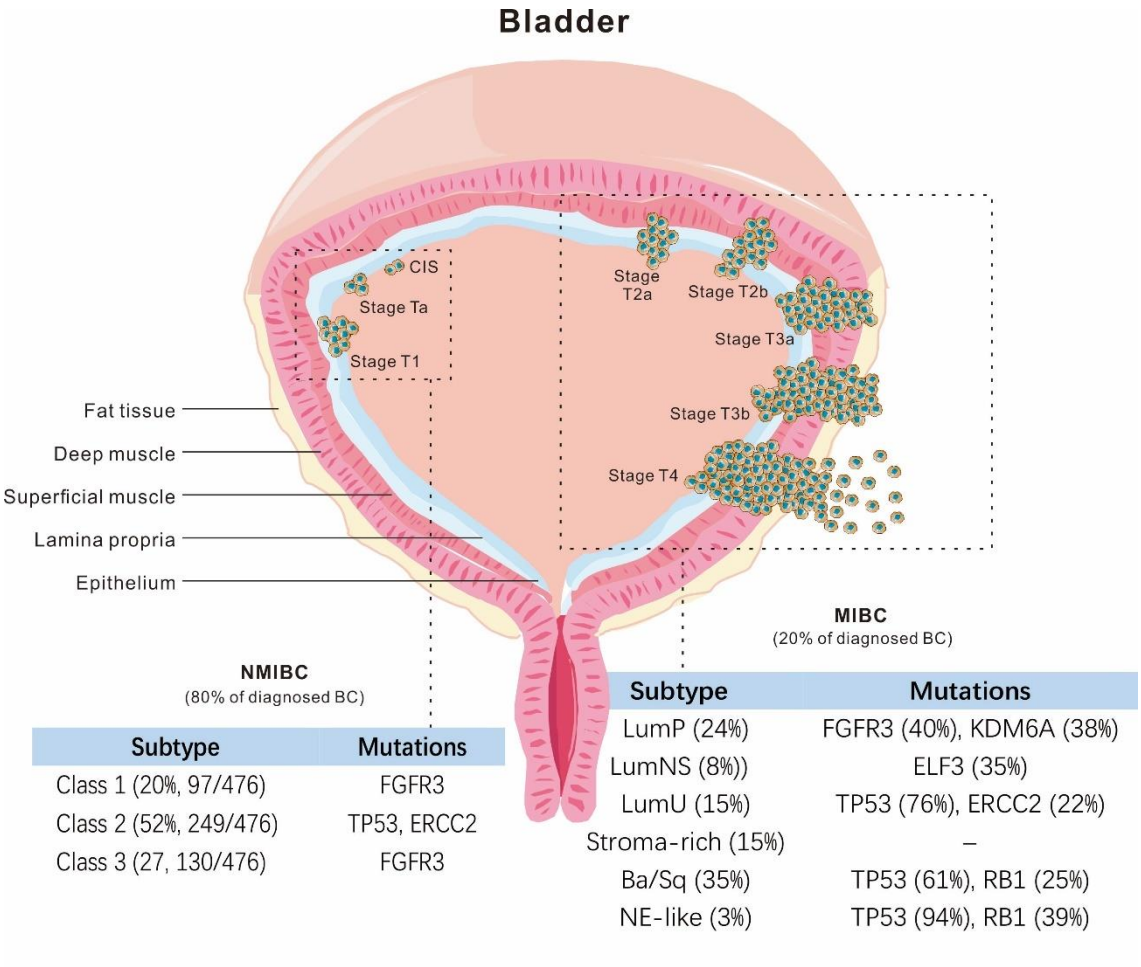

Figure 1.1.2: Clinical stages and molecular subclasses of bladder cancer. Bladder cancers are comprised of two subtypes: non-muscle-invasive bladder cancer (NMIBC) and muscle-invasive bladder cancer (MIBC). The NMIBC can be further classified into three subclasses, while MIBC can be classified into six subclasses. FGFR3, fibroblast growth factor receptor 3; TP53, tumor protein 53; ERCC2, excision repair cross-complementing rodent repair deficiency, complementation group 2; KDM6A, lysine demethylase 6A; ELF3, E74 like ETS transcription factor 3; RB1, RB transcriptional corepressor 1.

1.2 mTOR and Hsp90

1.2.1 PI3K/Akt/mTOR signaling pathway and mTOR inhibitors for cancer therapy

Mechanistic target of rapamycin (mTOR) is a serine-threonine kinase that has critical roles in cell survival, metabolism, proliferation, and autophagy [18, 19]. The mTOR mainly functions as a core component of two distinct protein complexes: mTOR complex 1 (mTORC1; comprised of mTOR, Raptor, and mLST8) and mTORC2 (mTOR, Rictor, and mLST8). The two mTOR-containing complexes are involved in different biological processes. mTORC1 mainly detects changes in oxygen levels, nutrient status and growth factors, while mTORC2 mainly senses changes in growth factors even under extreme conditions [20]. Moreover, mTORC1 inhibits ULK1-mediated autophagy [21]. Since mTOR pathway is involved in various signaling pathways during cell survival, the mTOR signaling pathway is important in tumor research. Dysregulation of mTOR pathways has been found to contribute to tumorigenesis, including bladder cancer. In many independent studies, it has been found that the mTOR pathway is over-activated in MIBC [22]. In addition, mutations in PIK3CA are present in 21–25% of MIBC.

Many rapamycin analogs (rapalogs) have been tested in clinical trials against many different types of human cancer: non-small cell lung cancer, endometrial cancer, advanced gastric cancer, hepatocellular carcinoma, and bladder cancer (ClinicalTrials.gov database). In bladder cancer, therapeutic effect was limited in various tested cell lines [23, 24]. The possible explanations for the limited effect are various, including failure to block all mTOR substrates [25], activation of the negative feedback on PI3K/Akt signaling [26], and induction of autophagy which acts as a protective role for cancer cells survival [27]. Torin2, a second generation ATP-competitive inhibitor of mTOR, is capable of targeting both complexes, which more completely inhibits mTOR [28]. This type of mTOR inhibitors may be promising in cancer therapy.

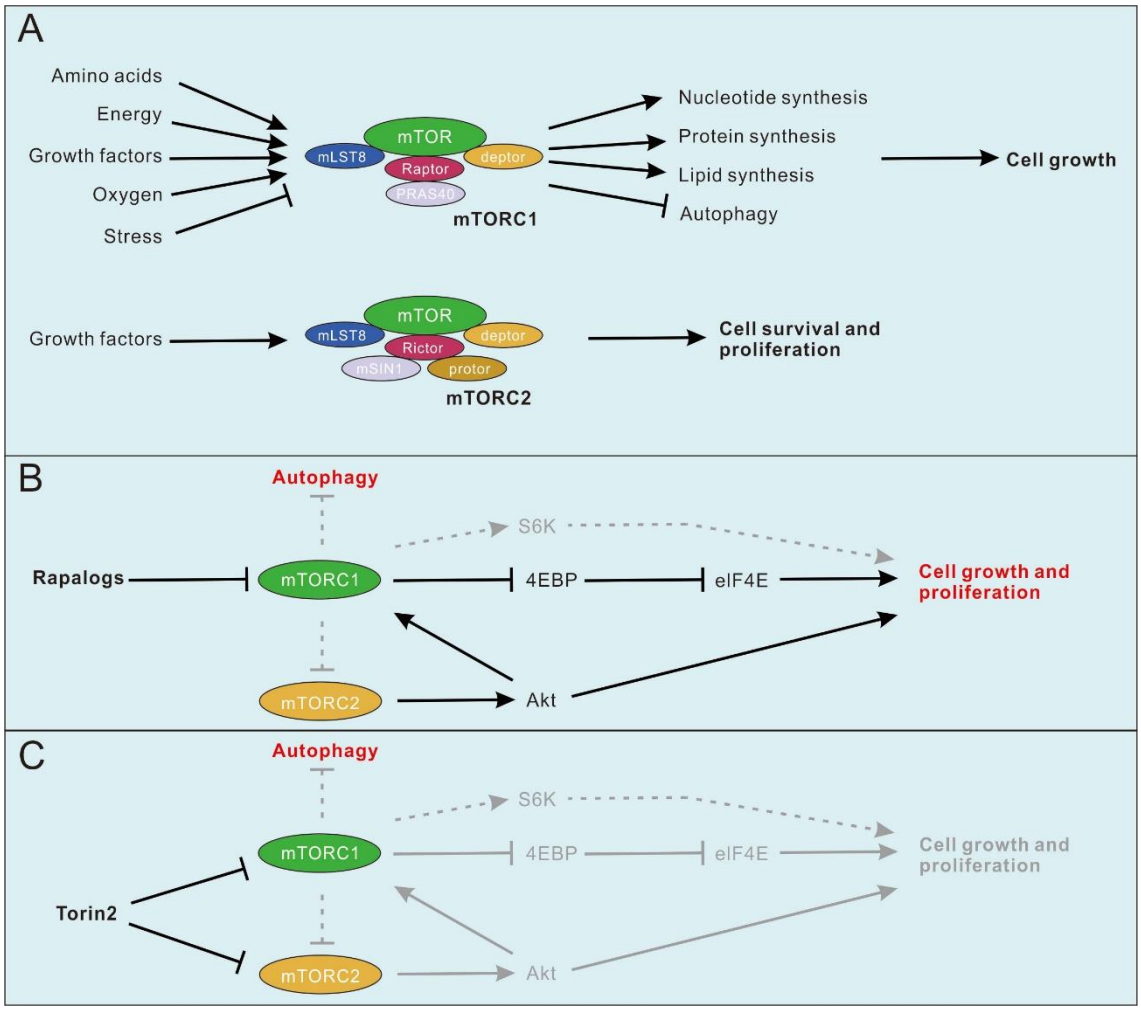

Figure 1.2.1: mTOR signaling pathways and the effects of rapalogs and Torin2. (A) mTOR signaling pathways. The mTORC1 complex is mainly comprised of mTOR, Raptor, and mLST8. The mTORC2 complex is mainly comprised of mTOR, Rictor, and mLST8. The two mTOR complexes sense different stimulations in cells and promote cell growth and proliferation. (B) mTOR signaling changes after rapalog treatment. Rapalogs fail to completely inhibit mTOR pathway and a negative feedback loop is activated, which further increases the activity of mTORC1. (C) mTOR signaling changes after torin2 treatment. Torin2 completely inhibits mTOR pathway and more effectively inhibits cell growth and proliferation. The red color names represent the activation of cellular processes.

1.2.2 Hsp90 protein and Hsp90 inhibitors for cancer therapy

Heat shock protein 90 (Hsp90), a molecular chaperone with over 200 identified client proteins, plays an essential role in ensuring correct protein folding and intracellular trafficking of its client proteins [29, 30]. The Hsp90 family is comprised of Hsp90α and Hsp90β in cytoplasmic, TRAP1 in mitochondria, and Grp94 in endoplasmic reticulum [31]. Hsp90 protein is a homodimer. Each monomer comprises of three domains: the N-terminal domain that contains an ATP binding pocket, co-chaperone interaction motifs, and drug binding sites; the middle domain that provides docking sites for co-chaperones and client proteins; and a C-terminal domain that contains drug binding sites and a dimerization motif by which the two monomers combine together [32]. Based on the research of the structure of Hsp90, nucleotide dependent conformational cycles have been proposed [33]. Briefly, Hsp90 begins in an open state with N-terminal opening. The binding of ATP in the ATP pocket of the N terminus shifts the conformation from an open structure to a closed structure. The hydrolysis of ATP causes the release of nucleotide and restarts the cycle. Many Hsp90 inhibitors are designed according to this conformational cycle.

Various of Hsp90 client proteins are known oncogenes, which is why Hsp90 inhibitors are used as cancer chemotherapeutic agents by inducing depletion of these clients [34]. While Hsp90 functions as a core component of the Hsp90 chaperone machinery, more than 12 distinct co-chaperones have been identified so far, which assist Hsp90 throughout its ATPase cycle and refolding of client proteins [35, 36]. Among these co-chaperones, cell division cycle 37 (Cdc37), first identified as a cell cycle protein [37], is a kinase-specific co-chaperone mediating the majority of interactions between kinase client proteins and Hsp90 [38]. Cancer cells utilize the Hsp90 chaperone machinery to protect a series of mutated and over-expressed oncoproteins from misfolding and degradation [39]. The malignant cells have higher proliferation rates and immortal tendency than normal cells, which allows them to survive under a stressful environment [40]. In addition, compared to normal cells, cancer cells are more sensitive to Hsp90 inhibition as they

strongly depend on oncogenes, which means they require higher level of Hsp90 than non-cancer cells [41, 42]. Since Hsp90 is a tub regulator for stress response pathways, looking for effective Hsp90 inhibitors has become one of the hot spots in cancer research. In cancer cells, Hsp90 presents in an activated chaperone complex which is hypersensitive to Hsp90 inhibitors [43].

Hsp90 inhibitors can be directed against different parts of Hsp90. There are two mainly types of Hsp90 inhibitors available, “classical” N-terminal inhibitors and C-terminal inhibitors. N-terminal inhibitors, such as 17-N-allylamino-17-demethoxygeldanamycin (17-AAG), have been widely tested under clinical trials in various cancers. However, the therapeutic effects of N-terminal inhibitors are not very satisfactory [44, 45]. The reasons for the low therapeutic efficiency of N-terminal inhibitors are various. Among them, the most important one is that the N-terminal inhibitors induce heat shock responses (HSR) while exerting its function, which causes the disassociation of heat shock factor 1 (HSF1) from Hsp90 and further activation of it [46, 47]. The promotion of survival by HSF1 overwhelms the inhibitory effect of Hsp90 inhibitors, which further weakens their effects. In contrast, C-terminal Hsp90 inhibitors do not cause HSR [48, 49]. The ability of these compounds to inhibit Hsp90 function without the consequence of HSR induction addresses one of the drawbacks of N-terminal inhibitors and makes C-terminal inhibitors interesting candidates for future development and cancer therapy.

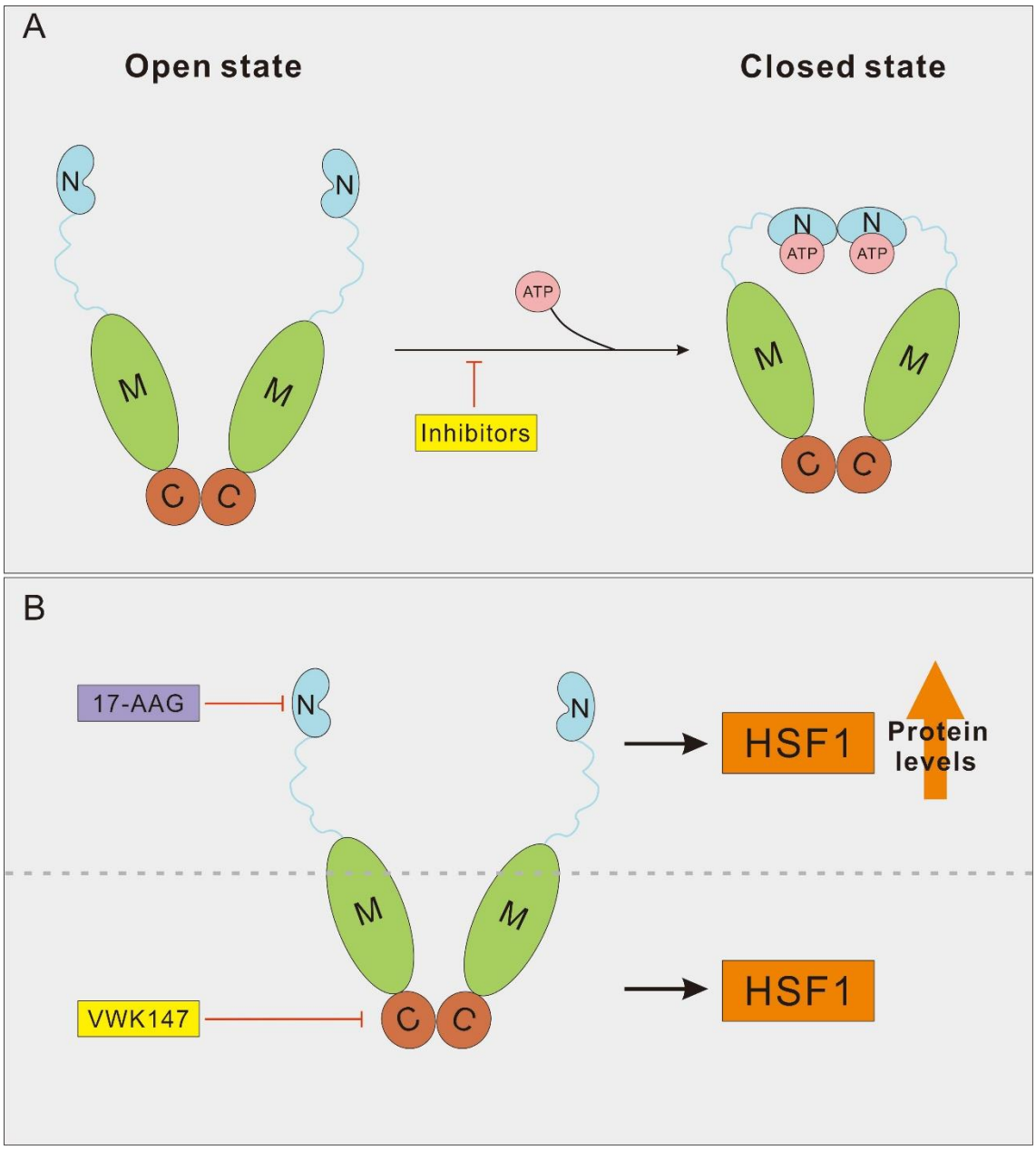

Figure 1.2.2: Conformational structure of Hsp90 and mechanism for two types of Hsp90 inhibitors. (A) Hsp90 begins in an open state with N-terminal opening. The binding of ATP in the ATP pocket of the N terminus shifts the conformation from an open structure to a closed structure. The hydrolysis of ATP causes the release of nucleotide and restarts the cycle. Hsp90 inhibitors function in the conformation cycle. (B) The N-terminal inhibitor 17-AAG induces HSR and further increases the protein level of HSF1, thereby reducing its cytotoxicity. The C-terminal inhibitor VWK147 does not induce HSR.

1.3 Autophagy

1.3.1 Autophagic signaling pathway

Autophagy is one of the biological processes responsible for intracellular renovation and protein degradation. Autophagy plays a very important “housekeeper” role in transporting unfolded proteins and damaged organelles into lysosomes to be degraded and recycled [50, 51]. This process is highly conserved in all eukaryotes, and can be activated by various stress conditions like the depletion of amino acids, glucose, oxygen, and growth factors. In addition, this orchestrated process ensures that the cells cope with different stress conditions by providing enough energy to cells. Therefore, autophagy is essential to maintain the balance between cell death and survival, and the dysregulation of autophagy often relates to various human diseases, including neurodegeneration and cancers [52].

Three different types of autophagy have been described in cells so far, which are macroautophagy, microautophagy and chaperone-mediated autophagy (CMA). Among them, CMA is a process in which proteins containing the KFERQ-motif are selectively recognized and degraded [53]. Microautophagy represents a process in which endosomes or lysosomes directly engulf autophagic cargo without involving autophagosomes as a means of transport [54]. Macroautophagy (hereafter referred to as autophagy) is the third but the best-investigated form of autophagy, in which special structures called autophagosomes surround and transport autophagic cargos into lysosomes [55]. This mechanism usually consists of a series of events related to the formation and development of autophagosomes, fusion with lysosomes and final degradation. Since macroautophagy is most relevant to this thesis, the following introduction of signaling pathway mainly focuses on it.

Macroautophagy is mediated by a number of autophagy-related (ATG) proteins and can be further divided into non-selective or selective autophagy, which are conducted through different signaling pathways. Generally, the autophagy processes comprise several stages: autophagy initiation, membrane nucleation and phagophore formation, phagophore

expansion or maturation, fusion with the lysosome and degradation. Each stage is conducted by different ATGs. The initiation stage is mainly regulated through the unc-51-like autophagy activating kinase 1 (ULK1) protein kinase complex, consisting of ULK1 itself, autophagy-related protein 13 (ATG13), focal adhesion kinase family interacting protein of 200 kDa (FIP200) and ATG101 [56]. The ULK1 complexed is mainly regulated by two upstream regulators: AMP-activated kinase (AMPK, positive regulator) and mTOR (negative regulator). These two upstream regulators sense cellular stress changes and further phosphorylate the ULK1 complex to regulate autophagy initiation. Once the ULK1 complex is activated by upstream regulators, it translocates to the autophagosome formation sites where the phosphatidylinositol synthase (PIS) is enriched [57]. The core effector for the next step of autophagy is the class III PtdIns3K complex, of which Beclin 1 (BECN1) and ATG14 are ULK1 substrates. Being directly phosphorylated by ULK1 and activated, the class III PtdIns3K complex I catalyzes the generation of PtdIns3P and recruits further downstream effector proteins [58, 59].

Following the class III PtdIns3K complex I activation and PtdIns3P production, downstream effectors of the WIPI protein family (mainly WIPI1, WIPI2 and WIPI4) are recruited and act as a bridge for PtdIns3P production and LC3 lipidation [60]. There are two ubiquitin-like conjugation systems that are essential for the expansion of autophagosomal membranes: ATG12 conjugation system (also known as ATG12–ATG5–ATG16L1 complex) and ATG8/LC3 conjugation system (including ATG3 and ATG7) [61]. Briefly, synthesized as a prosomal, ATG8 family proteins are subsequently cleaved by the protease ATG4 and a C-terminal glycine residue is exposed (ATG8-I, or LC3-I). With the help of two conjugation systems, ATG8 family proteins are conjugated to the lipid phosphatidylethanolamine (PE). This lipid form of ATG8 (ATG8-II or LC3-II) is present on autophagic membranes. Notably, the ATG8 family consists of microtubule-associated protein 1 light chain 3 (LC3) and gamma-aminobutyric acid receptor associated protein (GABARAP).

Following the closure and maturation of autophagosomes, the cargo inside of the autophagosomes is delivered to lysosomes for degradation and recycling. The fusion of

autophagosomes and lysosomes is regulated by soluble N-ethylmaleimide-sensitive-factor attachment receptor (SNARE) proteins [62]. Subsequently, autophagic cargos are degraded in autolysosomes.

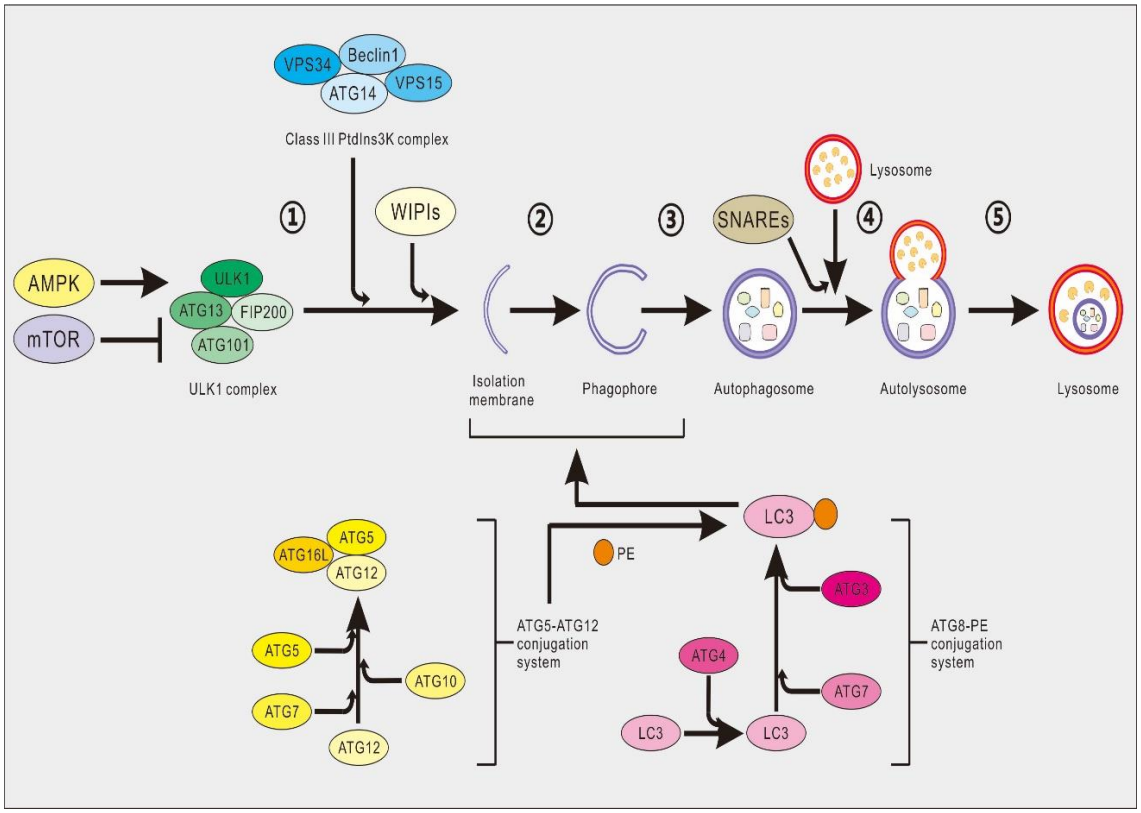

Figure 1.3.1: Main regulatory machinery of macroautophagy. The macroautophagy process mainly comprises five stages: 1. Autophagy initiation; 2. Membrane nucleation and phagophore formation; 3. Phagophore expansion or maturation; 4. Fusion with the lysosome; 5. Degradation of the engulfed cargo. ULK1 complex is activated by upstream regulators, it translocates to the autophagosome formation sites and phosphorylates the class III PtdIns3K complex. Following the class III PtdIns3K complex I activation, WIPIs are recruited and act as a bridge for PtdIns3P production and LC3 lipidation. LC3 lipidation is mediated by two ubiquitin-like protein complexes, which further promote autophagosome maturation. Autophagosome and lysosome fusion is mediated by SNAREs. Thereafter, the cargo is degraded in lysosomes and recycled as material for other cellular processes.

1.3.2 Autophagy in cancers

Since its important role in recycling intercellular harmful materials and maintaining cells at a stable station under stress conditions, autophagy is thought to be related to the proliferation and growth of cancers [63]. However, the relationship between autophagy and cancer is rather complex. To date, it is assumed that autophagy prevents cancer development. In turn, once cancer is established, the activation of autophagy and the increase in autophagy flux may benefit the survival and growth of cancer cells [64]. In addition, recent studies showed that the influence of autophagy on cancers is highly context-dependent [65]. As a multiple step process, autophagy can be inhibited or activated at different steps, including targeting the ULK1 complex, the class III PtdIns3K complex and lysosome fusion and protein degradation. Lysosome-targeting drugs such as chloroquine (CQ) or hydroxychloroquine (HCQ) are moving one step forward as potential compounds. It has been reported that these two compounds showed a good ability to inhibit tumor cells growth in clinical trials against various cancers [66, 67]. According to the results, the combination of HCQ and other chemotherapeutics showed good therapeutic effects in phase I clinical trials, and further stimulates research in phase II trials. In addition, autophagy inhibitors targeting other steps such as ULK1, PI3KC3 and ATG4B are under preclinical evaluation in mouse models and show promising anti-tumor effects in these approaches [68–70]. Although the mechanism is not fully understood, targeting autophagy might be a promising approach to cope with cancers.

1.3 Aims of thesis

Nowadays, bladder cancer is becoming a heavy economic burden in the EU. The therapeutic effects for bladder cancer are far from satisfactory. Cisplatin-based chemotherapy has been the first line treatment for advanced BC since the late 1980's. There are several drawbacks of the current cisplatin-based chemotherapy against bladder cancer, including drug toxicity, low response rates and cisplatin resistance. Therefore, there is an urgent need to find methods to reduce the side-effects of cisplatin and resensitize cisplatin-resistant cancer cells to cisplatin treatment.

This work aimed for exploring and evaluating other chemotherapeutic reagents against bladder cancer cells, especially regarding cisplatin-resistant cells. The effects of mTOR and Hsp90 inhibitors should be analyzed using immunoblotting in BC cell lines J82, 253J, T24, RT-112 and corresponding cisplatin-resistant counterparts. The cell viability of cisplatin-sensitive and -resistant BCs upon treatment with mTOR inhibitors, HSP90 inhibitors and combinations thereof should be analyzed in this thesis.

The following specific questions will be answered in this thesis:

1. Is the mTOR inhibitor Torin2 a good choice to cope with bladder cancer cells?
2. Are Hsp90 inhibitors suitable for use as anti-tumor reagents against bladder cancer?
3. Is there any difference between N-terminal and C-terminal Hsp90 inhibitors when used in combination with an mTOR inhibitor against bladder cancer cells?

2. Materials and Methods

2.1 Materials

All chemicals and biologically reactive reagents used in this thesis were purchased from Carl Roth (Karlsruhe, Germany), GE Healthcare (Chalfont St Giles, UK), Merck Millipore (VWR, Burlington, MA, USA), Sigma Aldrich (St. Louis, MO, USA), Thermo Fisher Scientific (Gibco, Molecular Probes, Waltham, MA, USA). All chemicals were purchased in p. A. quality unless otherwise indicated.

2.1.1 Oligonucleotides for siRNA knockdown

siRNA	Supplier and reference number (#)
ON-TARGETplus Human ULK1 siRNA SMARTpool	Dharmacon, # L-005049-00-0010
ON-TARGETplus Non-targeting Pool	Dharmacon, #D-001810-10-05

2.1.2 Compounds and supplements

Compounds and supplements	Supplier and reference number (#)
alamarBlue™ reagent	ThermoFisher, #DAL1100
Bafilomycin A_1	Sigma-Aldrich, #B1793
BL 918	Biosynth Carbosynth, # BB165666
Cisplatin	Accord Health care GmbH, PZN:00370955
DAPI	Carl Roth, #6335.1
DMSO	Sigma-Aldrich, #D4540
LYN-1604	Selleckchem, #S8597
ProLong™ glass antifade mountant	Invitrogen, #P36984
Torin2	Selleckchem, #S2817

Triton X - 100	Carl Roth GmbH & Co., #3051.2
17-AAG	Sigma-Aldrich, #A8476

VWK147 was kindly provided by Prof. Thomas Kurz (Institute for Pharmaceutical and Medicinal Chemistry, Faculty of Mathematics and Natural Sciences, Heinrich Heine University Düsseldorf).

2.1.3 Antibodies

Primary antibodies

All antibodies used for immunoblotting in this thesis were supplied by Abcam (Cambridge, UK), Bio-Rad (Hercules, CA, USA), Cell Signaling Technology (Danvers, MS, USA), Jackson ImmunoResearch (Cambridgeshire, UK), LI-COR Biosciences (Lincoln, NE, USA), MBL International (Woburn, MA, USA), Progen Biotechnik (Heidelberg, Germany), Santa Cruz Biotechnology (Dallas, TX, USA) or Sigma-Aldrich (St. Louis, MO, USA).

Antibody	Supplier and reference number (#)	Application
Rabbit anti-ULK1	Cell Signaling Technology, #8054	IB
Rabbit anti-ULK1 pSer757	Cell Signaling Technology, #6888	IB
Rabbit anti-ATG14	MBL, #PD026	IB
Rabbit anti-ATG14 pSer29	Cell Signaling Technology, #92340	IB
Guinea pig anti-SQSTM1/P62	Progen, GP62-C	IB
Rabbit anti-Hsp90	Cell Signaling Technology, #4875	IB
Rabbit anti-CDC37	Cell Signaling Technology, #4793S	IB
Rabbit anti-AKT	Cell Signaling Technology, #9272	IB
Rabbit anti-CDK4	Abcam, #ab108357	IB
Rabbit anti-C-RAF	Cell Signaling Technology, #53745	IB
Rabbit anti-LC3B	Cell Signaling Technology, #2775	IB

Mouse anti-α-Tubulin	Sigma-Aldrich, #T5168	IB
Mouse anti-GAPDH	Abcam, #ab8245	IB
Mouse anti-ACTB	Sigma-Aldrich, #A5316	IB
Rabbit anti-LC3B	MBL, #PM036	IF
Mouse anti-WIPI2	Biorad, #MCA5780GA	IF

Secondary antibodies

Antibody	Supplier and reference number (#)	Application
Goat anti-mouse IRDye®680RD	LI-COR Biosciences, #925-68070	IB
Goat anti-rabbit IRDye®680RD	LI-COR Biosciences, #925-68071	IB
Goat anti-mouse IRDye®800CW	LI-COR Biosciences, #926-32210	IB
Goat anti-rabbit IRDye®800CW	LI-COR Biosciences, #926-32211	IB
Donkey anti-guinea pig IRDye®680LT	LI-COR Biosciences, #925-68030	IB
Donkey anti-goat IRDye®680LT	LI-COR Biosciences, #926-68024	IB
Goat anti-rabbit Alexa Fluor® 488	Jackson ImmunoResearch, #111-545-003	IF
Goat anti-mouse Alexa Fluor® 647	Jackson ImmunoResearch, #115-605-003	IF

2.1.4 Buffers and solutions

Buffer	Solution
TRIS/HCL	0.5 - 1.5 M Tris; pH adjusted to 6.8 - 8.8 with HCl
1 x TBS	150 mM NaCl; 50 mM Tris
4% PFA in PBS	PFA dissolved in PBS using NaOH, pH adjusted to 7.0 with HCl

2.1.5 Media and supplements for cell cultruring

Media and supplements	Supplier and reference number (#)
Beta-mercaptoethanol	Sigma-Aldrich, #M3148
DMEM (4.5 g/L D-Glucose)	Thermo Fisher Scientific, #41965-039
DPBS (1x)	Thermo Fisher Scientific, #14190-094
EBSS	Thermo Fisher Scientific, #24010-043
Fetal Calf Serum (FCS)	Thermo Fisher Scientific, #10270
Trypsin/EDTA solution (0.05% / 1x)	Thermo Fisher Scientific, #25300-054

2.1.6 Additional materials

Media and supplements	Supplier and reference number (#)
Digitonin	Wako, 043-21376
DNA Gel loading dye (6x)	Thermo Fisher Scientific, #R0611
Dounce homogenizer	Wheaton
Glass cover slips, 10 mm	Paul Marienfeld, #0111500
Lipofectamine® RNAiMAX transfection reagent	Thermo Fisher Scientific, #13778
Neubauer counting chamber	Paul Marienfeld
PAGERuler TM Prestained Protein Ladder	Thermo Fisher Scientific, #26616
Polybrene	Sigma-Aldrich
Protease Inhibitor Cocktail	Sigma-Aldrich
PVDF membrane (Immobilon-FL)	Merck Millipore, #IPFL00010
Tissue culture equipment (dishes, pipettes etc.	Greiner, Sarstedt, Nunc

2.1.7 Laboratory equipment

Instrument	Supplier
Cell culture bench, HERAsafe®	Thermo Fisher Scientific

Cell culture incubator, HERAcell® 240 CO2	Thermo Fisher Scientific
Centrifuge, Heraeus™ fresco™ 17	Thermo Fisher Scientific
Centrifuge, Heraeus™ pico™ 17	Thermo Fisher Scientific
Centrifuge, Megafuge 40R	Thermo Fisher Scientific
Heating block (MBT 250)	Kleinfeld Labortechnik
LSM 710 inverse confocal laser scanning microscope with a Plan Apochromat 63x/1.4 oil objective	Zeiss
Microplate reader Synergy MX	BioTek
Milligram balance, MSE1203S-100-DE	Sartorius
Mini Electrophoresis system, Mini-PROTEAN Tetra	Bio-Rad
Odyssey® Infrared Imaging System I	LI-COR Biosciences
pH Meter, Five Easy	Mettler Toledo
Rotaiting Wheel	Neolab
Skaking unit, Duomax 1030	Heidolph
Thermomix comfort	Eppendorf
TSP SP2 inverse confocal laser scanning microscope with a Plan APO 63x water objective	Leica
Ultrasonic homogenizers, Sonoplus HD 2070	Bandelin
Wet transfer unit	Bio-Rad

2.1.8 Software and suppliers

Software	**Supplier**
Adobe Acrobat Reader 11.0	Adobe System Inc, USA
CorelDraw® X7	Corel Corporation, Canada
GraphPad PRISM 7	GraphPad Software, USA
ImageJ	Rasband, USA
Image Studio Light V.4	LI-Cor, USA
Microsoft® Office 2016	Microsoft Corporation, USA

ZEN 3.0 (blue edition)	Zeiss, Germany

2.1.9 Websites and databases

https://gco.iarc.fr/

https://blast.ncbi.nlm.nih.gov/Blast.cgi

http://www.ncbi.nlm.nih.gov

http://www.uniprot.org

2.2 Methods

2.2.1 Cell culture

MEFs and Cisplatin sensitive BCs.

Cell culture work was performed under a laminar flow cell culture bench. All cell lines were cultured in Dulbecco's Modified Eagle Medium (DMEM) supplemented with 10% fetal calf serum (FCS) at 37°C in a humidified atmosphere containing 5% CO_2. FCS was inactivated of complement factors by heating it to 56 °C for 30 minutes prior to use. Cells were passaged when confluent. For cell passaging, old medium was discarded and cells were washed with 1 x PBS once and treated with prewarmed trypsin for five minutes until cells detached from the bottom of flasks or dishes. Trypsinization was stopped by adding 3 times the volume of medium. Cells were harvested using a refrigerated centrifuge at 1500 rpm for 3 minutes, and the pellet was resuspended in medium.

Cisplatin resistant BCs

Cisplatin-sensitive and -resistant cell lines J82, 253J, T24 and RT-112 were provided by Margaretha Skowron (Department of Urology, Heinrich Heine University Düsseldorf,

Germany). Cisplatin-resistant cells were cultured under constant presence of cisplatin (1, 2, 7, and 15 µg/ml for J82, 253J, T24, and RT-112 cells, respectively).

2.2.2 Cell freezing and thawing

Cell freezing medium was set up by contained 90% (v/v) FCS and 10% (v/v) DMSO. For cell freezing, old medium was discarded and cells were washed with 1 x PBS once and detached with prewarmed trypsin for five minutes. Trypsinization was stopped by adding 3 times the volume of medium. Cells were harvested using a refrigerated centrifuge at 1500 rpm for 3 minutes, and the pellet was resuspended in freezing medium. 1 mL cell suspension was transferred into a ctyo-tube and frozen at -80 °C. For long term storage, the cells were transferred into liquid nitrogen. For cell thawing, the cells were warmed in a 37 °C water bath, immediately transferred into prewarmed medium and cultured in the 37 °C incubator.

2.2.3 Cell viability assay (alamarBlue assay)

2.2.3.1 Reagents preparation

NaCl / Pi buffer:	0.1497 g KH_2PO_4 (1.1 mM); 8.99 g NaCl (154 mM); 0.525 g Na_2HPO_4 (3.7 mM). The above mixture was filled up to 1 L with ddH_2O and stored at 4 °C.
AB stock solution: (8.8 mM)	0.22 g of resazurin was weighted and dissolved in 100 ml ddH_2O. After complete dissolving, the solution was filtered through a 0.45 µm syringe filter for sterilization. The filtered solution was wrapped with aluminum foil and frozen in 10 ml aliquots at 20 °C.
AB 10 x working solution: (440µM)	2.5 ml of alamarBlue stock solution was added to 47.5 ml NaCl / Pi buffer in a 50 ml aluminum foil

falcon tube.

2.2.3.2 Assay procedures

When cells were in log phase of growth, they were harvested and the cell number was determined. The cell density was adjusted to 1×10^5 cells/ml with medium. 0.5×10^4 cells (in 50 µl medium) were seeded in 96-well pates. The following day, the cells were treated with 50 µl of different concentrations of compounds for 72 hours. There were 3 replicates of each concentration to minimize technical errors. After the indicated time, 10 µl of alamarBlue reagent was added to cells in culture medium and incubated at 37°C without direct light for 4 hours. After the incubation time, the fluorescence was measured with excitation wavelength at 560 nm and emission wavelength at 590 nm. The fluorescence was detected by using a microplate reader (BioTek, Synergy Mx).

2.2.3.3 Assay controls setting

Negative control:	No cells, only medium and alamarBlue reagent
Untreated control:	Cells, medium and alamarBlue reagent
Positive control:	200 mM of tested compounds (Torin2 or Hsp90 inhibitors)

2.2.3.4 Calculation of results

% Reduction of alamarBlue =

$$\frac{(\text{Experimental RFU value} - \text{Untreated Control RFU value}) \times 100}{\text{Positive control RFU} - \text{Untreated control RFU value}}$$

% Difference between T & UT=

$$\frac{\text{Experimental RFU value with test compound} \times 100}{\text{Untreated Control RFU value}}$$

RFU: fluorescence reading

2.2.4 Western blot

2.2.4.1 Cell lysis and protein isolation

Cells were harvested by scraping, collected and pelletized at 1200 rpm for 5 minutes. The cell pellets were washed once with DPBS and recentrifuged at 1200 rpm for 5 minutes. Afterwards, the pellets were resuspended and lysed in an appropriate volume of ice-cold lysis buffer (LB) for 30 minutes on ice. The lysates were vortexed every 5 minutes. After lysis time ends, the lysates were centrifugated at 18, 000 g and 4 °C for 15 minutes to spin down insoluble fragments and nuclei. The supernatant was then transferred to new 1.5 ml eppendorf tubes and the concentration of total protein
was measured (see 2.1.4.2).

Lysis buffer	20 mM Tris / HCl, pH 7.5, 150 mM NaCl, 0.5 mM EDTA, 1% [v/v] Triton X – 100, 1 mM Na_3VO_4, 10 µM Na_2MoO_4, 2.5 mM NaPP, 10 mM NaF and protease inhibitor cocktail

2.2.4.2 Total protein concentrations measurement

Bradford method was used to measure protein concentration, which is a spectroscopic assay for aqueous protein solutions. This assay was performed in 96-well format.

Reagents preparation

Bradford reagent	Dilute 5 x Bradford stock 1:5 in ddH_2O
BSA standard	0, 50, 100, 150, 200, 250, 300, 400 µg/ml in DPBS

Assay procedures

Samples were set up in duplicates by mixing 10 µl of CCLs (dilution range 1:10 to 1:100)

with 200 µl Bradford reagent. The absorbance of each sample was detected at 595 nm (Biotek, Synergy MX) after 5 minutes incubation at room temperature. Protein concentration was calculated according to the BSA standard curve. The protein concentrations were adjusted to 25 µg total protein per 20 µl using lysis buffer containing 6 x SDS sample buffer.

2.2.4.3 SDS polyacrylamide gel electrophoresis (SDS-PAGE)

SDS-PAGE is an electrophoresis method that allows protein separation according to their molecular weight. The method is composed of sample preparation, gel preparation, electrophoresis, gel staining and analysis. Acrylamide gel is composed of an upper layer stacking gel and a lower layer separating gel, which concentrates the protein samples and separates the proteins by mass separately. The final concentrations of separating gels were from 10% to 15%, depending on the molecular weight of the individual proteins. 15% gels were used to detect protein sizes ranging from 12 kDa to 45 kDa, while 10% gels to detect protein sizes in the range of 15 – 100 kDa. The final concentration of stacking gels used in this thesis is always 5%. CCLs samples were heated at 95 °C for 5 minutes and then loaded on gels together with a molecular weight marker (Thermo Fisher Scientific). The gels were placed in SDS running buffer and a constant current of 40 mA was applied. The electrophoresis process lasts one hour. Thereafter, gels were subjected to immunoblot analysis (see 2.1.4.4).

6 x SDS sample buffer	375 mM Tris/HCl; 25.8% (v/v) glycerol; 12.3% (w/v) SDS; 6% (v/v) β-ME; 0.06% (w/v) bromophenol blue
SDS running buffer	250 mM Tris; 19 M glycine; 0.1% (w/v) SDS
Stacking gel	1.0 M Tris/HCl, pH 6.8; 5% acrylamide; 0.74% (w/v) SDS; 0.1% TEMED; 0.1% APS
Separating gel	1.0 M Tris/HCl, pH 8.8; 6-15% acrylamide;

	0.38% (w/v) SDS; 0.1% TEMED; 0.1% APS

2.2.4.4 Immunoblot analysis

After the completion of SDS-PAGE, the proteins were transferred to polyvinylidene fluoride (PVDF) membranes to further detect proteins by specific antibodies. Prior to use, PVDF membranes were activated in MeOH for 1 minute. Blotting was performed in transfer buffer at a constant voltage of 100 V for 1 h at 4 °C. After completed transfer, the membranes were soaked in blocking buffer for 1 hour under constant agitation. Thereafter, membranes were washed three times with TBS-T for 5 min and incubated with primary antibodies at 4 °C over night under constant agitation. The primary antibodies were diluted in TBS-T containing 0.05% NaN_3 from 1:1,000 to 1:20,000 according to the manufacturer's instructions. The following day, membranes were washed three times using TBS-T for 5 minutes and incubated with secondary antibodies (1:20,000 in TBS-T) in opaque boxes for 1 hour at room temperature under constant agitation. Afterwards, membranes were washed three times with TBS-T for 5 min and dried between blotting papers. After being completely dried, the membranes were analyzed using an Odyssey® Infrared Imaging System I (LI-COR Biosciences) and densitometry was performed using Image Studio Light Version 4 (LI-COR Biosciences).

Transfer buffer	43.58 mM Tris; 39 mM glycine
TBS-T	0.05% (v/v) Tween® 20 in TBS
Blocking solution	5% (w/v) skimmed milk in TBS-T

2.2.5 Immunofluorescence

2.2.5.1 Reagents preparation

Fixation buffer	4% (w/v) formaldehyde in PBS, adjusted

	pH to 6.9
Permeabilization buffer	5% (w/v) digitonin in PBS
Blocking solution	3% (w/v) BSA in PBS

2.2.5.2 Assay procedures

6×10^4 cells were plated on 12 mm round glass cover slips. The following day, the cells were treated with indicated compounds for 4 hours. Subsequently, the cells were washed once with PBS and fixed using 4% paraformaldehyde (PFA) for 15 minutes on ice. For quenching the free aldehyde groups, the cells were incubated with 50 mM NH_4Cl for 15 minutes at room temperature. After washing three times with PBS, the cells were permeabilized with 50 µg/ml Digitonin for 5 minutes at room temperature. Again, the cover slips were washed three times with PBS and incubated with 3% BSA/PBS for 30 minutes at room temperature. The blocking solution was tapped off the cover slips and diluted primary antibodies (1:100 in 3% BSA/PBS) were added on the cover slips. After one hour of incubation in a dark and humidified chamber, the cover slips were washed three times with PBS and incubated with diluted secondary antibodies (1:500 in BSA/PBS) for 1 hour at room temperature in the dark. The cover slips were washed twice with 0.2% Tween and then washed twice with PBS. Afterwards, the cells were mounted on a glass slide using Prolong Gold Antifade Reagent with DAPI (1 µg/ml). The cover slips were then imaged using Zeiss Axio Observer 7 (ApoTome extension, Objective Plan-Apochromat 40x/1,4 Oil DIC M27). Quantification of puncta and analyses of immunofluorescence were performed by using ImageJ software.

2.2.6 siRNA-mediated gene knockdown

Cells were transfected with siRNA against ULK1 and control siRNAs at 50 nM final concentration using DharmaFECT reagent according to the manufacturer's instructions. Briefly, 1.5×10^6 cells/ml were seeded in 6-well plates. The following day, the medium

was exchanged to fresh medium 1 hour before transfection. A mixture containing 192.75 µl of optiMEM with 7.25 µl of siRNA was prepared and incubated for 5 minutes at room temperature. Meanwhile, another mixture of 196 µl of optiMEM with 4 µl of DharmaFECT 1 bzw. Duo was prepared and incubated for 5 minutes at room temperature. Both solutions were then mixed and incubated for additional 20 minutes at room temperature. Afterwards, medium was removed from cells and 400 µl of mixed solution was added to the cells. The knockdown efficiency was detected by using western blot assay after 48 hours of incubation.

2.2.7 Statistical analysis

For the quantification of western blots, the density of each protein band was divided by the average value of all bands of the same protein on the membrane. Afterwards, the ratios of proteins were normalized to corresponding loading controls, and fold changes were calculated by dividing each normalized ratio by the average of the ratios of the control lane. IC50 values were calculated using GraphPad Prism 7.01. CompuSyn 1.0 was used to calculate Combination index (CI) and perform isobologram analysis. CI values indicate antagonism ($CI > 1$), additive effect ($CI = 1$), synergism ($CI < 1$). All experiments were performed independently at least three times. Data were statistically compared by GraphPad Prism 7.01, and P values were determined using one-way ANOVA or two-way ANOVA.

3. Results

3.1 Cisplatin resistant bladder cancer cells tolerate higher concentrations of cisplatin than sensitive cells

J82, 253J, T24 and RT-112 cell lines were used in this thesis to represent the heterogeneity, clinical stages and pathological grades. The historical data of each cell line was collected, such as gender, stage, grade and PMID (Figure 3.1.1).

Cell line	Gender	Stage	Grade	PMID
J82	male	pT3	G3	687519
253J	male	pT4	G4	4431054
T24	female	pTa	G3	4133950
RT-112	female	pTa	G2	864752

Figure 3.1.1 Summary of BCs used in this thesis. The information search was conducted using PubMed on the published results of bladder cancer cell lines from 1980 to 2020.

Cisplatin resistant cell lines were generated by culturing cells in a cisplatin-containing medium for more than 3 months (see 2.2.1) and were kindly provided by Margaretha Skowron (Department of Urology, Heinrich Heine University Düsseldorf, Germany). In order to compare the cisplatin tolerance between different BCs, the four different cisplatin-resistant cell lines and their parental cells were used for alamarBlue analysis. In all pairs, in terms of IC_{50} values, the cisplatin tolerance of CRs was 5.6 - 13.3 times higher than that of its parental cells (Figure 3.1.2). Collectively, these data confirmed that CRs exhibit a distinctive nature and an increased tolerance to cisplatin treatment.

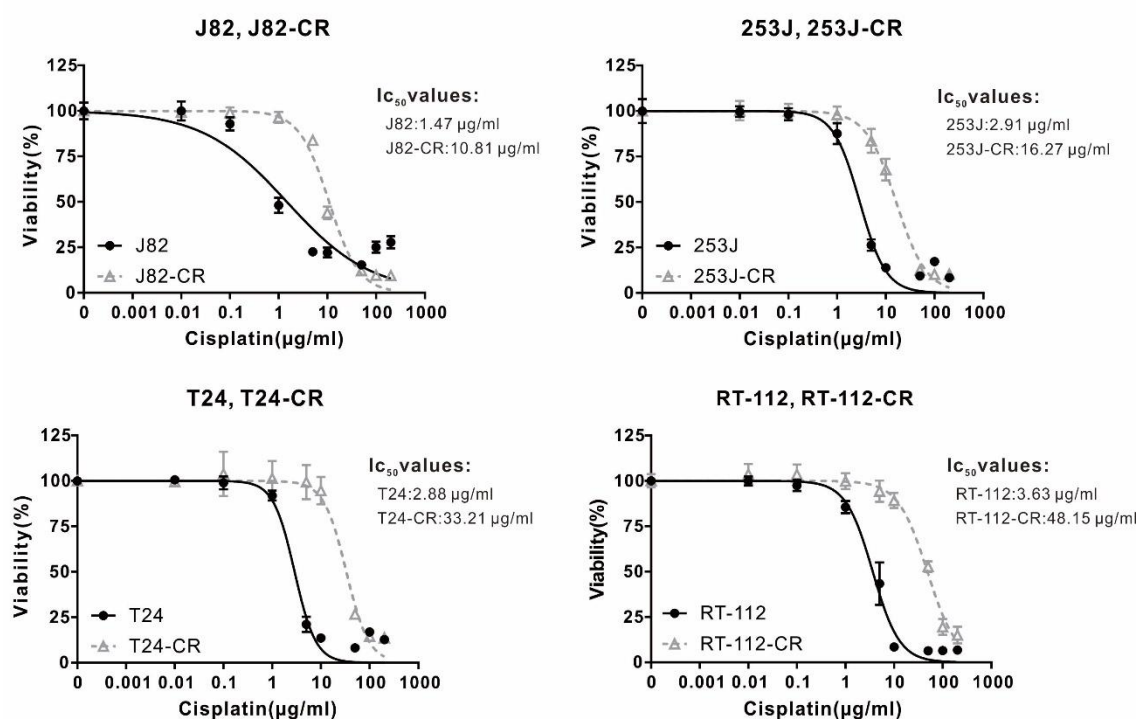

Figure 3.1.2: Characterization of four different cisplatin-sensitive and -resistant urothelial bladder carcinoma cell lines. The calculated IC_{50} values are indicated on the upper right corner of line charts. Cells were exposed to different concentrations of cisplatin (0.01-200 µg/ml) for 72 hours and cell viability was measured using alamarBlue assay. Values are expressed as means ± standard deviation ($n \geq 3$).

3.2 mTOR Inhibition decreases cell viability in both cisplatin-sensitive and -resistant BCs

The mTOR pathway is activated in up to 40% of bladder cancers, and its activation is closely related to tumor progression [71]. Therefore, targeting the Akt-mTOR pathway is a promising strategy for the treatment of advanced bladder cancer. Several mTOR inhibitors (such as everolimus, sirolimus and temsirolimus) are clinically applied alone or in combination with other drugs. The therapeutic effects of these inhibitors are variant in different tumors. Among all inhibitors, Torin2, a potent and selective mTOR inhibitor, has shown a powerful effect in inhibiting the two mTOR complexes. Therefore, it is used in this thesis. To confirm the effects of mTOR inhibition by Torin2 in BC cells, the mTOR substrate ULK1 was analyzed. Under nutrient sufficiency, high mTOR activity prevents

ULK1 activation by phosphorylating ULK1 Ser758 (corresponds to Ser757 in mouse) and disrupting the interaction between ULK1 and AMPK. As shown in figure 3.2.1, Torin2 decreased ULK1 phosphorylation at Ser758 in both T24 cisplatin-sensitive and -resistant cells. Given the fact that mTORC1-mediated phosphorylation of ULK1 prevents the activation of ULK1 [72] , ATG14 Ser29, a ULK1 substrate usually used as a readout for ULK1 activation, was upregulated after Torin2 treatment. Therefore, mTOR pathway was effectively inhibited by Torin2 in T24 cells.

In addition, compared with T24 cells, the autophagy-related proteins ULK1 and ATG14 were significantly up-regulated in T24-CR cells, suggesting that cisplatin resistant bladder cancer cells showed increased potential to execute autophagy.

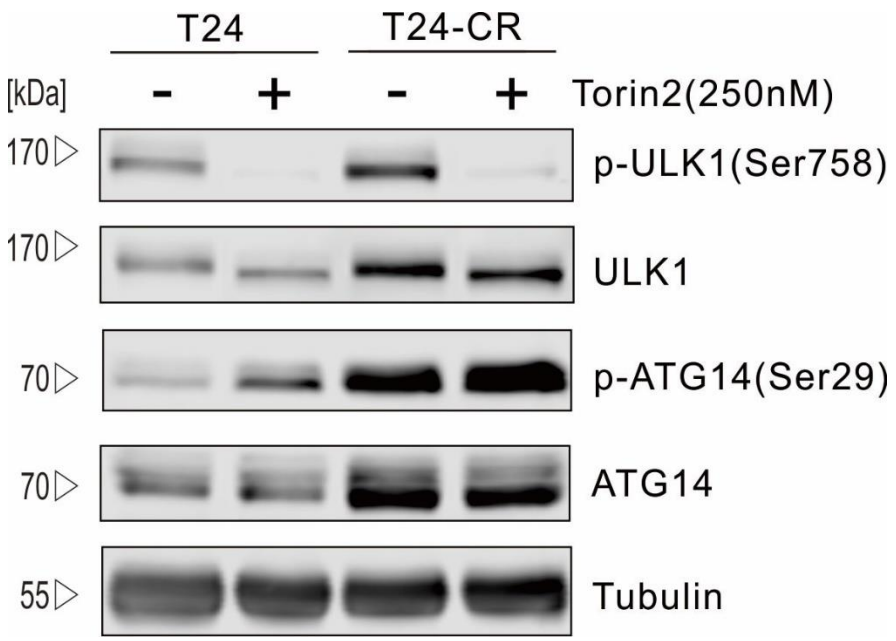

Figure 3.2.1: Torin2 effectively inhibits mTOR pathway in T24 and T24-CR cells. T24 and T24-CR cells were treated with or without 250 nM of Torin2 for 2 h. After indicated time, cells were lysed, subjected to SDS-PAGE and visualized by immunoblotting. α-Tubulin was used as a loading control.

Next, it was investigated whether mTOR inhibition by Torin2 affected cell viability in all four pairs of BCs. As indicated in figure 3.2.2, Torin2 showed high cytotoxicity in all tested cells. Noteworthy, in 253J and T24 pairs, the IC_{50} values of Torin2 in cisplatin resistant cells were lower than the ones of sensitive cells, indicating an increased

sensitivity of CRs against Torin2 treatment. Besides, 253J and T24 are derived from high pathological grades of bladder cancer (G4 and G3 respectively). In particular, 253J-CR, which represents the late stage of bladder cancer cells, showed good response to mTOR inhibitory treatment. This might provide us with a promising perspective for improving therapeutic outcomes of cisplatin-based chemotherapy against advanced bladder cancer.

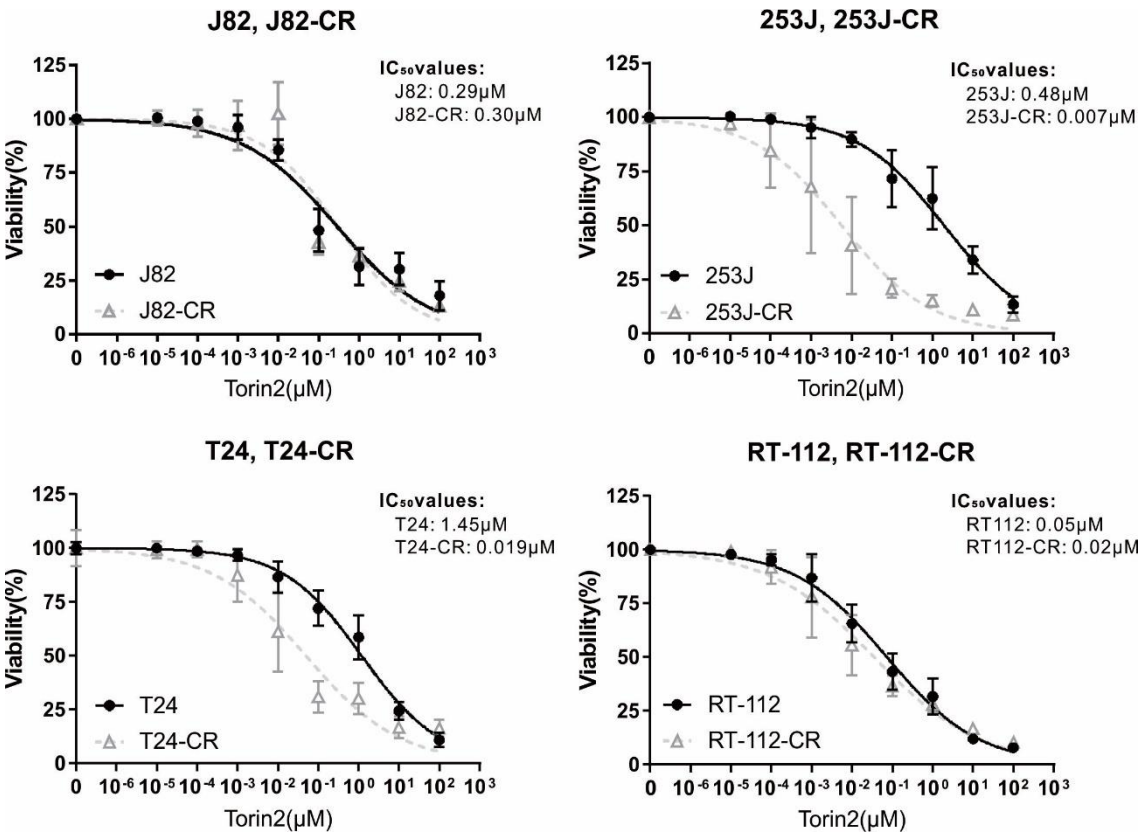

Figure 3.2.2: The mTOR inhibitor Torin2 is cytotoxic to BCs. The calculated IC_{50} values are indicated on the upper right corner of line charts. Cells were treated with different concentrations of Torin2 (0.01 nM-100 μM) for 72 hours and cell viability was measured using alamarBlue assay. Values are expressed as means ± standard deviation ($n \geq 3$).

3.3 N-terminal and C-terminal Hsp90 inhibitors decrease cell viability in cisplatin-sensitive and -resistant BCs

The heat shock protein 90 (Hsp90), a key regulator of protein homeostasis, stabilizes the

structural and functional integrity of client proteins [73]. It has been previously described that Hsp90 inhibitors enhance the anti-tumor effect of cisplatin against CRs [74]. To further investigate the effects of different types of Hsp90 inhibitors on cisplatin-sensitive and -resistant BCs, the expression level of Hsp90 in these cells was analyzed by immunoblotting. As showed in figure 3.3.1, unlike the expression of autophagy related proteins, the protein levels of Hsp90 remains similar in T24- and 253J-CRs and their parental BCs.

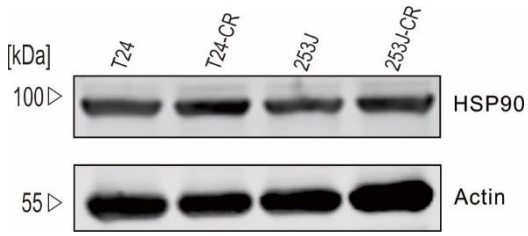

Figure 3.3.1: The protein levels of Hsp90 in different BCs. T24, T24-CR, 253J and 253J-CR cells were collected by scraping and lysed. 25 µg of total protein were loaded on the SDS-PAGE gels and analyzed by immunoblotting. The housekeeping protein β-Actin was used as loading control.

In order to evaluate the inhibitory effects of these two different Hsp90 inhibitors in BCs, some previously reported Hsp90 client proteins, such as c-Raf, RIPK1 and AKT, were used to evaluate whether these compounds can inhibit Hsp90 function in BCs. As shown in figure 3.3.2, the N-terminal inhibitor 17-AAG effectively decreased the abundance of clients using a relatively low doses (1 µM and 2 µM) in T24 and T24-CR cells.

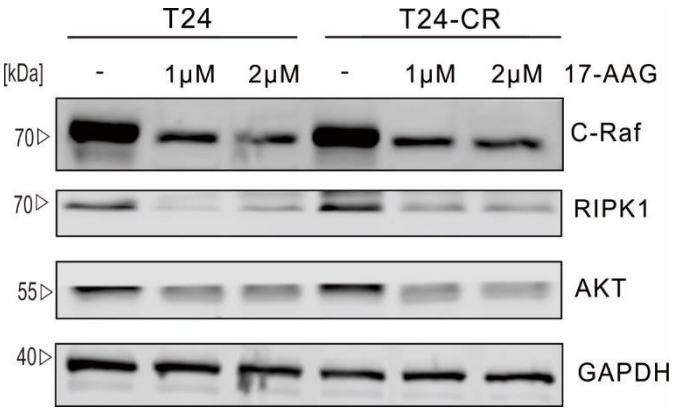

Figure 3.3.2: N-terminal inhibitor 17-AAG decreased the abundance of Hsp90 clients. T24 and T24-

CR cells were treated with DMSO or 17-AAG (1µM or 2µM) for 24 hours. After treatment, cells were collected by scraping and lysed. 25 µg of total protein were loaded on the SDS-PAGE gels and analyzed by immunoblotting. Samples were analyzed for c-Raf, RIPK1 and AKT. The housekeeping protein GAPDH was used as loading control.

Hsp90 inhibitors have been demonstrated as a promising targeted therapy regimen. Their therapeutic activity have been seen in melanoma, prostate cancer and breast cancer [75, 76]. To evaluated anti-tumor effects of 17-AAG in bladder cancer cells, cell viability was evaluated using alamarBlue assay after 72 hours of treatment of BCs with different concentrations of 17-AAG. As indicated in figure 3.3.3, 17-AAG showed high cytotoxicity in all tested cells, with IC_{50} in the range of 0.04-16.63 µM. Intriguingly, in all tested BCs, the IC_{50} values of 17-AAG in cisplatin resistant cells were lower than these in sensitive cells, indicating an increased sensitivity of CRs against 17-AAG treatment.

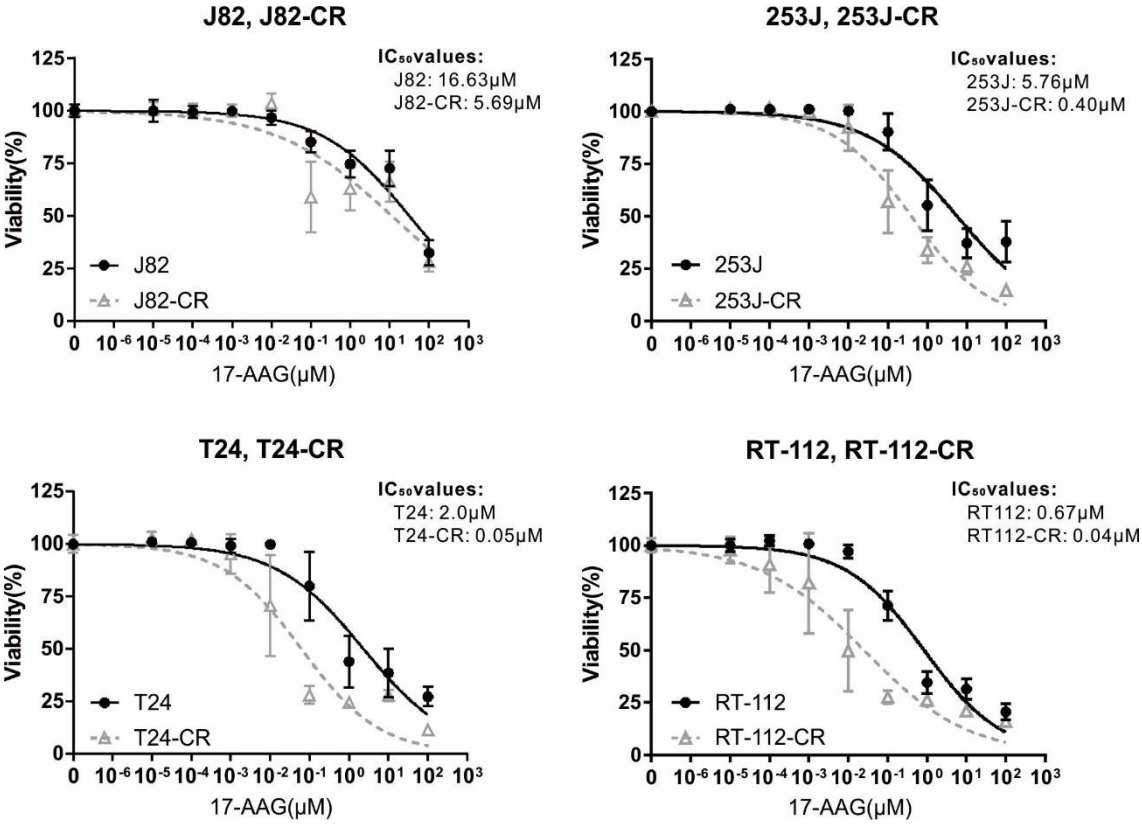

Figure 3.3.3: The N-terminal Hsp90 inhibitor 17-AAG is cytotoxic to BCs. The calculated IC_{50} values are indicated on the upper right corner of line charts. Cells were treated with different concentrations of 17-

AAG (0.01 nM-100 μM) for 72 hours and cell viability was measured using alamarBlue assay. Values are expressed as means ± standard deviation. (n ≥ 3).

The N-terminal inhibitors such as 17-AAG execute Hsp90 inhibition function mainly by targeting the adenosine triphosphate (ATP) binding pockets located in the N-terminus of Hsp90 [74]. However, the binding of the N-terminal ATP pocket can lead to the destruction of the Hsp90-shock factor-1 (HSF-1) interaction, which further promotes the translocation of HSF-1 into the nucleus, leading to increased expression of pro-survival components, such as Hsp7 and Hsp27. Increased abundance of these proteins induces a resistance mechanism named heat shock response (HSR), which attenuates the cytotoxic effects of Hsp90 inhibition [77–79]. In contrast, C-terminal inhibitors can avoid the induction of HSR. Therefore, they might be more promising than N-terminal inhibitors to maximize the effects of Hsp90 inhibition. In this thesis, the C-terminal inhibitor VWK147 (kindly provided by Prof. Thomas Kurz, Institute for Pharmaceutical and Medicinal Chemistry, Faculty of Mathematics and Natural Sciences, Heinrich Heine University Düsseldorf) was employed to compare whether the two inhibitors are different in Hsp90 inhibition and cytotoxicity against cisplatin-sensitive and -resistant BCs. Similar to the analysis described above, the Hsp90 inhibition effects of VWK147 was evaluated by immunoblotting using Hsp90 clients, such as c-Raf, RIPK1 and AKT. As shown in figure 3.3.4, N-terminal inhibitor VWK147 effectively decreased the abundance of clients in T24 cells.

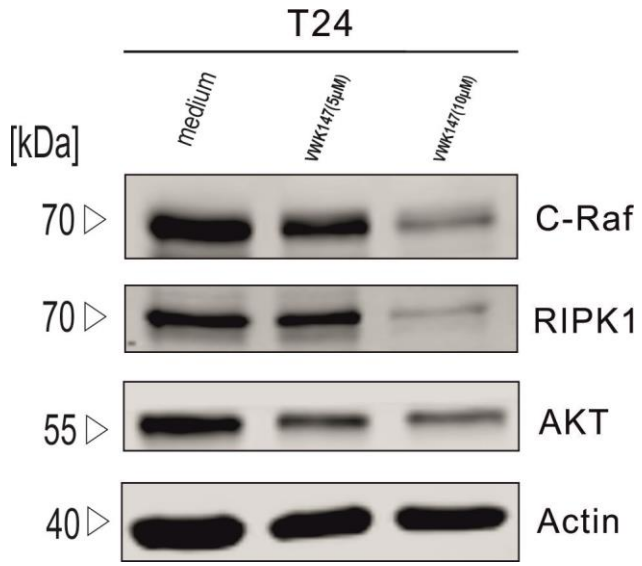

Figure 3.3.4: C-terminal inhibitor VWK147 decreased the abundance of Hsp90 clients. T24 cells were treated with DMSO, VWK147 (5μM or 10μM) for 24 hours. After incubation, cells were collected by scraping and lysed. 25 μg of total protein were loaded on the SDS-PAGE gels and analyzed by immunoblotting. Samples were analyzed for c-Raf, RIPK1 and AKT. The housekeeping protein Actin was used as loading control.

Next, the cell viability of T24 and T24-CR cells was evaluated by alamarBlue assay after 72 hours of treatment with different concentrations of VWK147. As shown in figure 3.3.5, VWK147 showed cytotoxicity to all 4 pairs of BCs. Noteworthy, 253J-CR and T24-CR cells were more sensitive to VWK147 than their parental cells, which is consistent to Torin2 treatment.

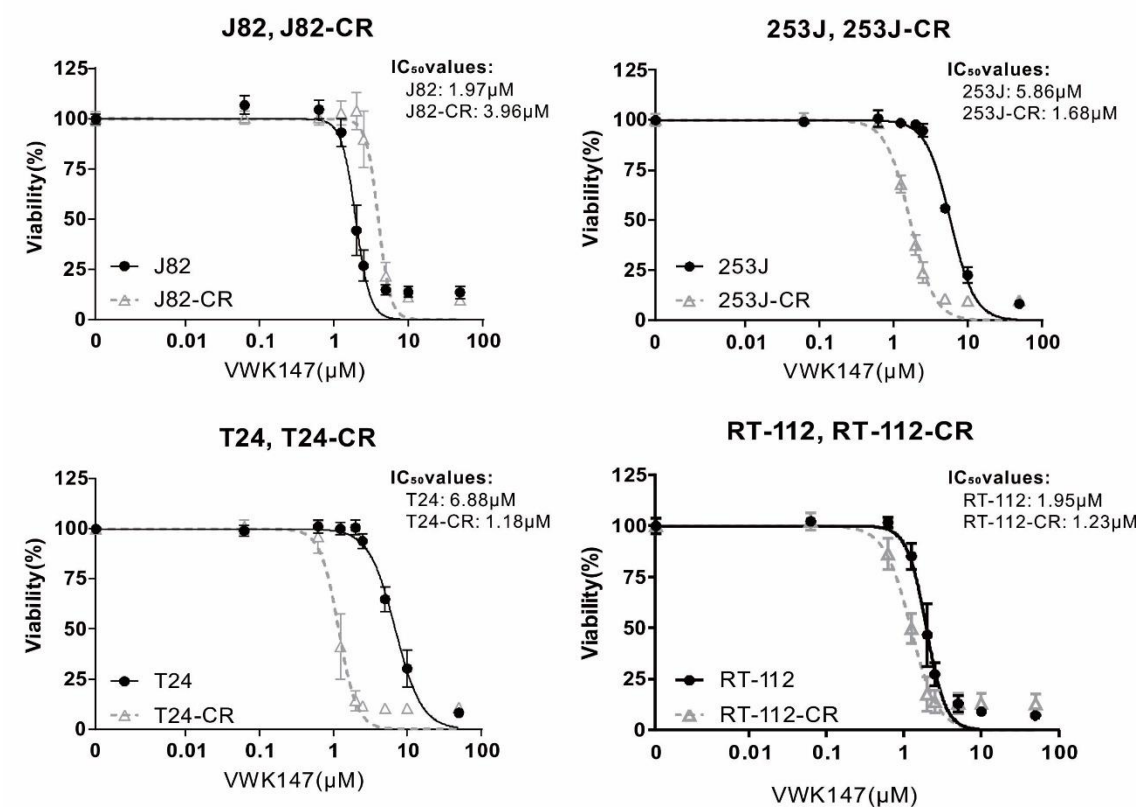

Figure 3.3.5: The C-terminal Hsp90 inhibitor VWK147 is cytotoxic to BCs. The calculated IC_{50} values are indicated on the upper right corner of line charts. Cells were treated with different concentrations of VWK147 (0.01 nM-100 μM) for 72 hours and cell viability was measured using alamarBlue assay. Values are expressed as means ± standard deviation. ($n \geq 3$).

Collectively, both N-terminal Hsp90 inhibitor (17-AAG) and C-terminal Hsp90 inhibitor (VWK147) effectively decreased the abundance of Hsp90 client proteins. When using 1 μM of 17-AAG, it was found that Hsp90 client proteins were obviously degraded, while treatment with 5 μM of VWK147 only showed a moderate decrease in the clients. Therefore, the N-terminal Hsp90 inhibitor 17-AAG showed higher efficiency than the C-terminal inhibitor VWK147 in destabilizing Hsp90 clients in BCs. In terms of cell viability experiments, both two inhibitors showed high cytotoxicity to BCs. Besides, cisplatin resistant BCs (253J-CR and T24-CR) were more sensitive to Hsp90 inhibitors than their parental cells, indicating Hsp90 inhibitor a promising reagent to improve cisplatin therapeutic effects to cisplatin-resistant BCs.

3.4 The combination of Torin2 and C-terminal Hsp90 Inhibitor is synergistic in cisplatin-sensitive and -resistant BCs.

The mTOR inhibitors have been widely examined in various cancer models, including breast cancer, lung cancer, gastric carcinoma, prostate cancer, and bladder cancer, etc [80]. However, the effects of mTOR inhibitors utilized as monotherapy in cancer are sometimes dampened by several resistance mechanisms [81]. Since many Hsp90 client proteins play a major role in the mTOR pathway, we therefore tested if Hsp90 inhibitors can sensitize BC cells towards mTOR inhibition. In order to investigate whether Torin2 and two HSP90 inhibitors exhibit a combined effect on cell viability in these two cell lines, the effects of these compounds treatment alone or combination were analyzed. As shown in figure 3.4.1, the combination of Torin2 and Hsp90 inhibitors showed higher cytotoxicity than the corresponding monotherapy. It can be concluded from the combination index graph that in T24 cells, if used at the 1x IC_{50} concentration of a single compound, the two HSP90 inhibitors work synergistically with Torin2 (CI <1). When the concentrations of 0.25 and 0.5× IC_{50} were used, the combined effects of Torin2 and VWK147 were synergistic, while 17-AAG exhibited an antagonistic effect with Torin2 (CI=4.8 and 16). 17-AAG and Torin2 were working synergistically when 2× IC_{50} was used, whereas VWK147 exhibited moderately antagonistic effect in combination with Torin2 (CI=1.5).

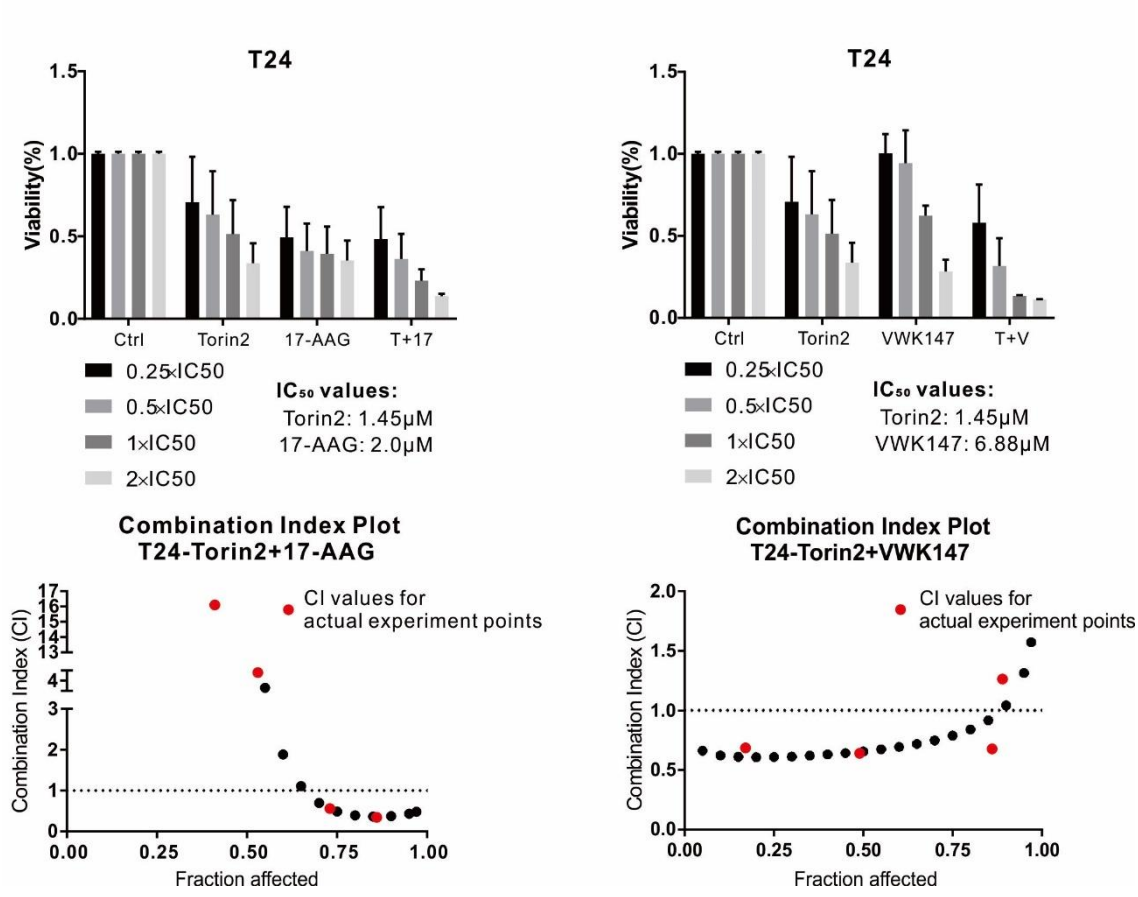

Figure 3.4.1: The combination effects of Torin2 and two Hsp90 inhibitors in T24 cells. T24 cells were treated with Torin2 combined with VWK147 or 17-AAG (0.25 ×, 0.5 ×, 1 × and 2 × IC_{50}) for 72 hours. The IC_{50} values of each compound were calculated based on the previous mono-treatment. The cell viability was measured using alamarBlue assay. The combination index values were calculated using software CompuSyn [82]. The actual experiment points were indicated as red dots whereas simulation dots processed by CompuSyn were indicated as black dots. The combination effects of Torin2 and VWK147 were determined synergistic (CI < 1), additive (CI = 1) and antagonistic (CI > 1). Values are expressed as means + standard deviation (n ≥ 3).

Next the combination effects were tested in T24-CR cells (figure 3.4.2). In T24-CR cells only the C-terminal Hsp90 inhibitor VWK147 acted synergistically (CI < 1) with Torin2 in the concentrations of 0.25 × ,0.5 × and 1 × of the IC_{50} values whereas N-terminal inhibitor 17-AAG worked antagonistic with Torin2 in all tested concentrations. This result indicates that when used in combination with mTOR inhibitor against CRs, the C-

terminal Hsp90 inhibitor has an advantage over the N-terminal one.

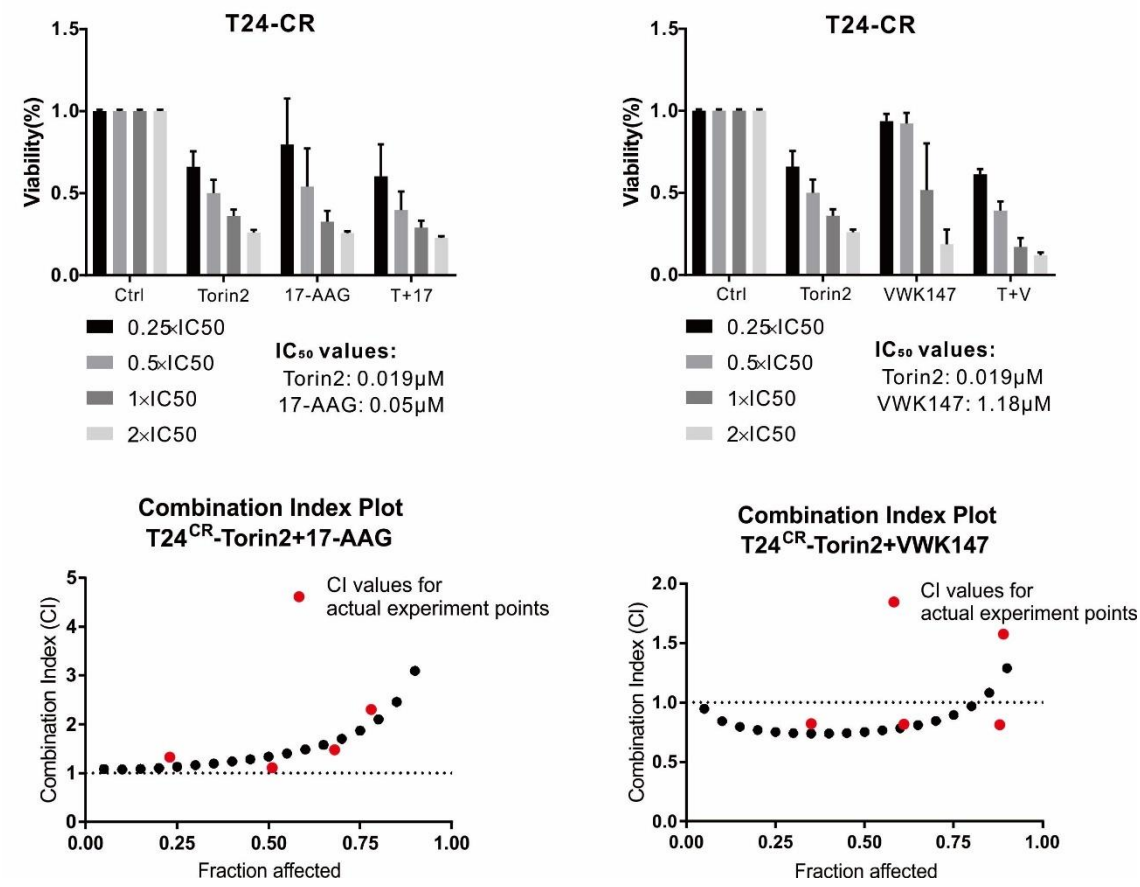

Figure 3.4.2: The combination effects of Torin2 and two Hsp90 inhibitors in T24-CR cells. T24-CR cells were treated with Torin2 combined with VWK147 or 17-AAG (0.25 ×, 0.5 ×, 1 × and 2 × IC_{50}) for 72 hours. The IC_{50} values of each compound were calculated based on the previous mono-treatment. The cell viability was measured using alamarBlue assay. The combination index values were calculated using software CompuSyn [82]. The actual experiment points were indicated as red dots whereas simulation dots processed by CompuSyn were indicated as black dots. The combination effects of Torin2 and VWK147 were determined synergistic (CI < 1), additive (CI = 1) and antagonistic (CI > 1). Values are expressed as means + standard deviation (n ≥ 3).

Moreover, the synergistic effects of Torin2 and VWK147 were confirmed in other BC cells. As shown in figure 3.4.3, when treated at concentrations of 0.25 × of the IC_{50} values, Torin2 and VWK147 acted synergistically in all tested BCs except for J82 cells. Further,

upon treatment with 0.5 × or 1 × IC_{50}, Torin2 and VWK147 had synergistic effects in all tested BCs. In summary, whether in cisplatin-sensitive or -resistant bladder cancer cells, Hsp90 inhibitor targeting C-terminus showed promising combined effects with mTOR inhibition. This might give a new perspective for chemotherapy and cisplatin resistance reversal of bladder cancer.

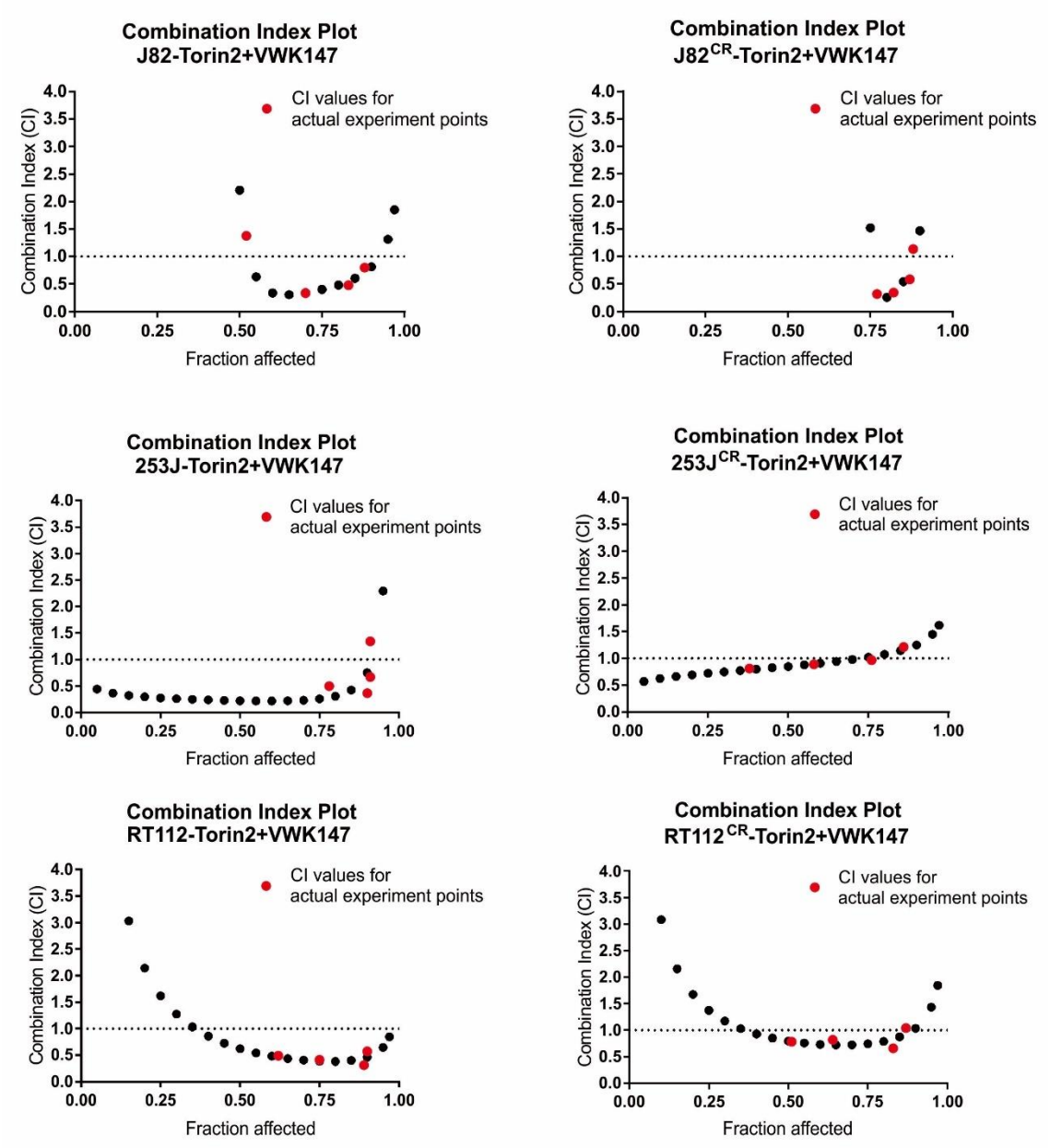

Figure 3.4.3: The combination effects of Torin2 and VWK147 in cisplatin-sensitive and -resistant cells.

Cells were treated with Torin2 combined with VWK147 (0.25 ×, 0.5 ×, 1 × and 2 × IC_{50}) for 72 hours. The IC_{50} values of each compound were calculated based on the previous mono-treatment. The cell viability

was measured using alamarBlue assay. The combination index values were calculated using software CompuSyn [82]. The actual experiment points were indicated as red dots whereas simulation dots processed by CompuSyn were indicated as black dots. The combination effects of Torin2 and VWK147 were determined synergistic (CI < 1), additive (CI = 1) and antagonistic (CI > 1).

3.5. The C-terminal Hsp90 Inhibitor VWK147 induces LC3 lipidation in bladder cancer cells.

Autophagy has been widely researched as a process by which misfolded and aggregated proteins are delivered to lysosomes for degradation [83]. Besides, many key proteins of autophagy, such as ULK1, BECN1 and GABARAP are clients of Hsp90. In this thesis, the effects of Hsp90 inhibition on autophagy pathway were researched. As shown in figure 3.5.1, ULK1, an important kinase needed in early steps of autophagosome biogenesis, was destabilized by both types of Hsp90 inhibitors.

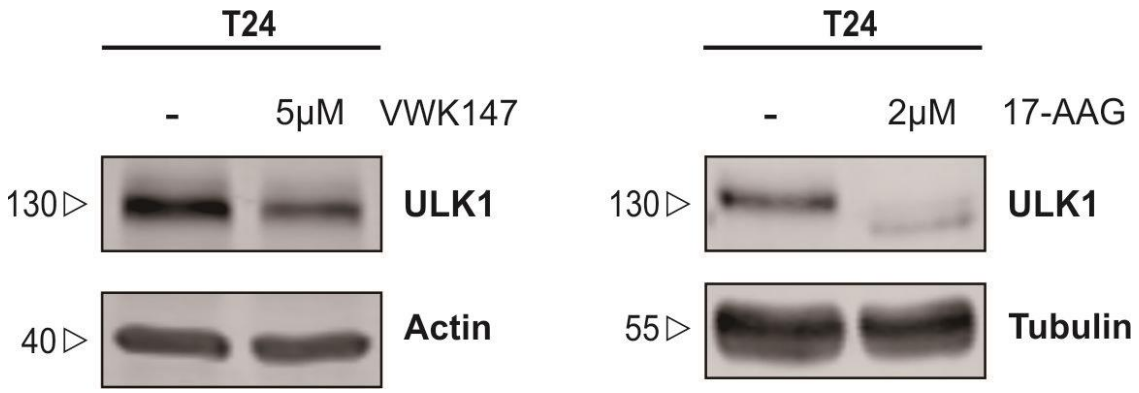

Figure 3.5.1: Hsp90 inhibitors decreases the abundance of ULK1. T24 cells were treated with DMSO, VWK147 (5μM) or 17-AAG (2μM) for 24 hours. After incubation, cells were collected by scraping and lysed. 25 μg of total proteins were loaded on the SDS-PAGE gels and analyzed by immunoblotting. Samples were analyzed for ULK1. The housekeeping proteins Actin or Tubulin were used as loading control.

Noteworthy, 17-AAG showed higher ability than VWK147 to destabilize ULK1, which was consistent with the former experiments. In addition, the ULK1 band shifted to a lower molecular weight after the treatment with 17-AAG, indicating that 17-AAG might affect the post -translational modification of ULK1. To further explore the effects of the C-terminal inhibitor VWK147 on ULK1 abundance and autophagy pathway, T24 cells were treated with different concentrations of VWK147 for 24 hours. The protein level of ULK1 and autophagy marker LC3 were detected using immunoblotting. VWK147 reduced ULK1 protein level in a dose-dependent manner (figure 3.5.2). Surprisingly, VWK147 also increased the LC3-II expression level, the lipidated form of LC3, in a dose-dependent manner.

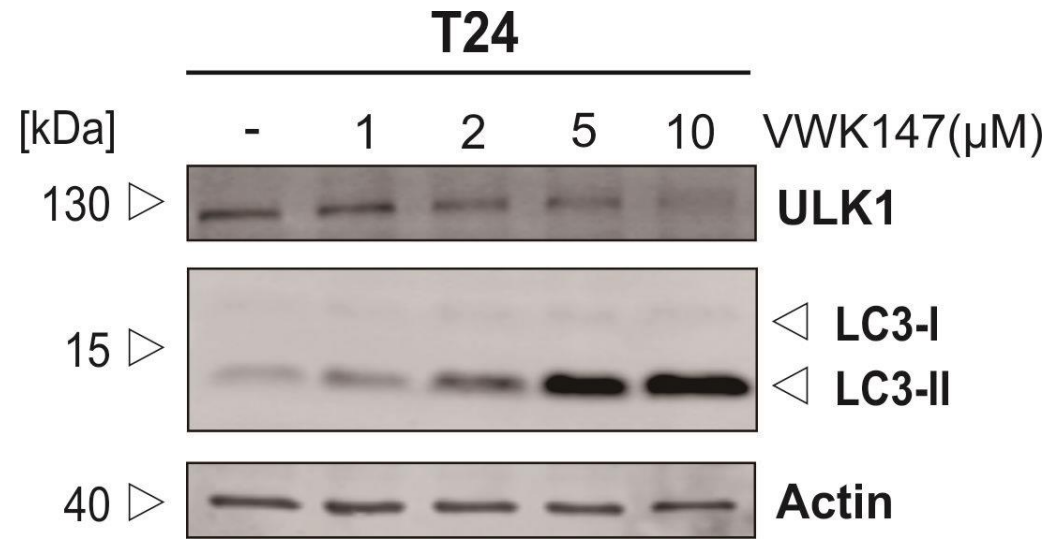

Figure 3.5.2: VWK147 decreases the abundance of ULK1 and increases LC3-II. T24 cells were treated with different concentrations of VWK147 for 24 hours. After incubation, cells were collected by scraping and lysed. 25 µg of total proteins were loaded on the SDS-PAGE gels and analyzed by immunoblotting. Samples were analyzed for ULK1 and LC3. The housekeeping protein Actin was used as loading control.

We then performed LC3 turnover assay to figure out whether increased LC3-II levels were due to induction of autophagy, disturbance of autophagosome-lysosome fusion or increase of LC3 lipidation. As indicated from the LC3 turnover analysis shown in figure 3.5.3, autophagy inhibition in these two cell lines could be excluded, since in both cells,

the amount of LC3-II was higher in the VWK147 + Baf.A1 group than that of the VWK147 group. Baf.A1 blocks the degradation of LC3-II, resulting in the accumulation of LC3-II. Accordingly, the differences in the amount of LC3-II between samples in the presence and absence of Baf.A1 represent the amount of LC3 that is delivered to lysosomes for degradation. Compared to VWK147 only, LC3-II increases in VWK147 + Baf.A1 indicates the amount of degraded LC3-II. In addition, the LC3-II levels in VWK147 + Baf.A1 was higher than Baf.A1 only, indicating newly synthesized LC3-II is also increased. In summary, VWK147 increases autophagosome flux. However, according to P62 turnover assay results, there were no decrease or increase of P62 level after VWK147 treatment, indicating autophagic substrate flux did not occur. Collectively, VWK147 induces LC3 lipidation or non-canonical autophagy in BCs.

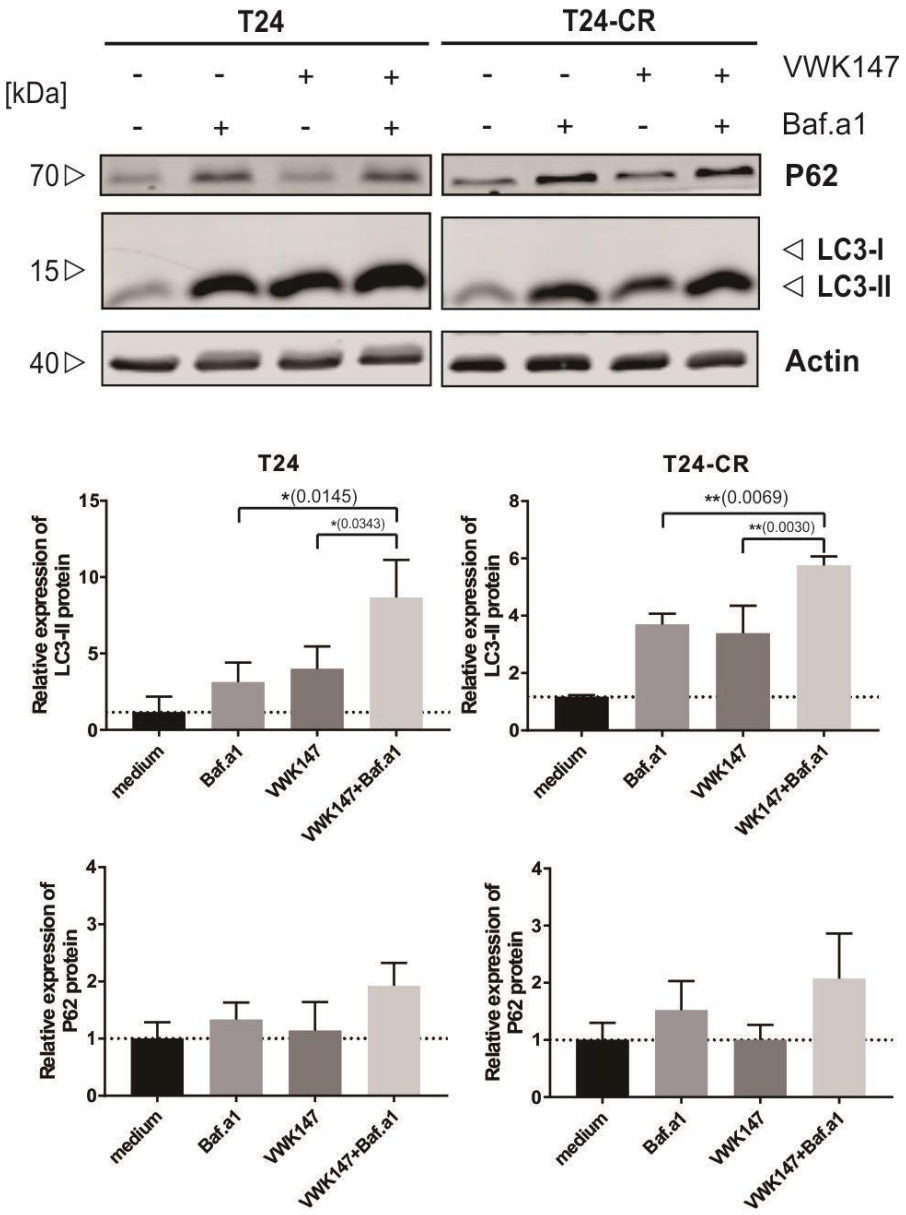

Figure 3.5.3: WB results for LC3 and P62 turnover assay. T24 and T24-CR cells were treated with Baf.A1 (20 nM), VWK147 (7 µM or 1.5 µM, i.e. approximate IC_{50} concentration, respectively) or Baf.A1+VWK147 for 4 hours. After incubation, cells were collected by scraping and lysed. 25 µg of total protein were loaded on the SDS-PAGE gels and analyzed by immunoblotting. Samples were analyzed for P62 and LC3. The housekeeping protein Actin was used as loading control. Histograms showed the results of quantification analysis of the protein bands above using Image Studio and normalized to the mean of each control values. The error bars represent the means + standard deviation (n=3).

To further explore whether autophagy was induced after VWK147 treatment, WIPI2, a

marker for early stages of autophagosome biogenesis was detected using immunofluorescence staining. In addition, EBSS was included as positive control. Compared to EBSS treatment, no significant increase of WIPI2 dots were found after VWK147 treatment. Besides, other autophagy markers such as ATG16L (early stages of autophagosome marker) and LAMP-1 (lysosome marker) were also investigated (see supplementary figures 6.2.1 and 6.2.2). Similar to WIPI2, no significant increase in the aggregation of ATG16L was observed. The results of WIPI2 and ATG16L indicated that there was no early stage autophagosome generation. Although the number of LAMP-1 aggregation was seen to increase, they were not colocalized with LC3, indicating other lysosome-involved cellular processes were induced by VWK147 but not autophagy. Furthermore, LC3 puncta were seen to increase after EBSS and VWK147 treatments. Compared to LC3 dots induced by EBSS, VWK147 induced larger LC3 positive structures. Collectively, these findings demonstrated that VWK147 treatment induced LC3 lipidation and accumulation in T24 and T24-CR cells.

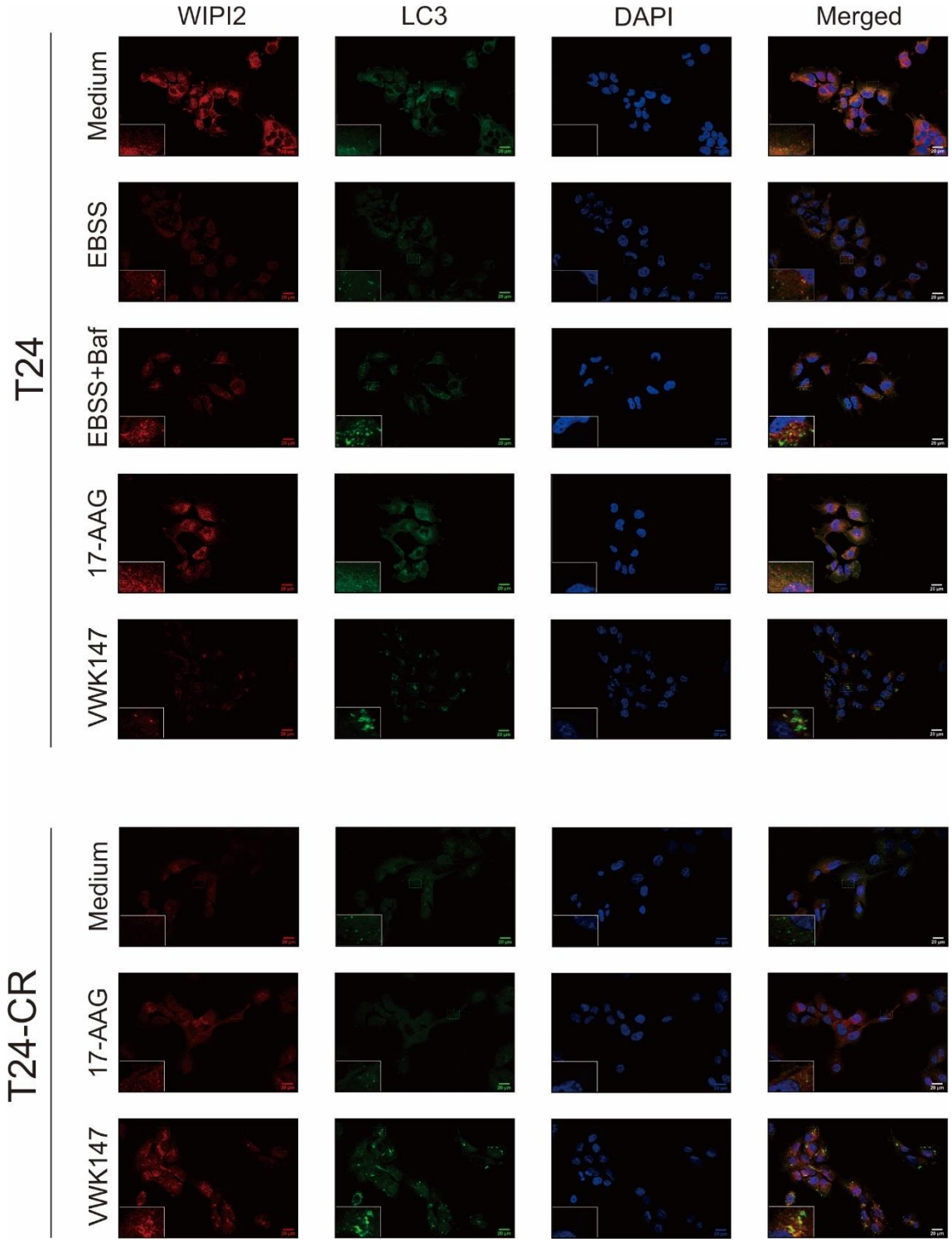

Figure 3.5.4: VWK147 does not induces WIPI2 puncta formation in T24 and T24-CR cells. T24 and T24-CR cells were treated with VWK147 (7 µM and 1.5 µM) or 17-AAG (2 µM) for 6 hours, and T24 cells were treated with EBSS or EBSS + Bafilomycin (20 nM) for 2 hours. After the treatment, cells were fixed, permeabilized and immunostained for WIPI2 and LC3. The Zeiss Axio Observer 7 fluorescence microscope (Zeiss, Köln, Germany) with a Plan Apochromat 40x/1.4 oil objective (Zeiss, Köln, Germany) was used for imaging. Nuclei were counterstained with DAPI. Scale bar: 20 µm.

3.6. The C-terminal Hsp90 Inhibitor VWK147 induced LC3 lipidation that is independent of ULK1 and PIK3C3.

Canonical LC3 lipidation is orchestrated by two ubiquitin- like conjugation systems during autophagy [84]. To further investigate the connection between the observed VWK147-induced LC3 lipidation and autophagy, the expression level of ULK1 was down regulated using siRNA. As shown in figure 3.6.1, ULK1 expression level was successfully downregulated in T24 and T24-CR cells. In addition, the phosphorylation of ATG14 at Ser29 was also decreased, indicating that the kinase activity of ULK1 was downregulated as well after ULK1 knockdown. However, VWK147-induced LC3 lipidation remained almost unaffected by ULK1 knockdown.

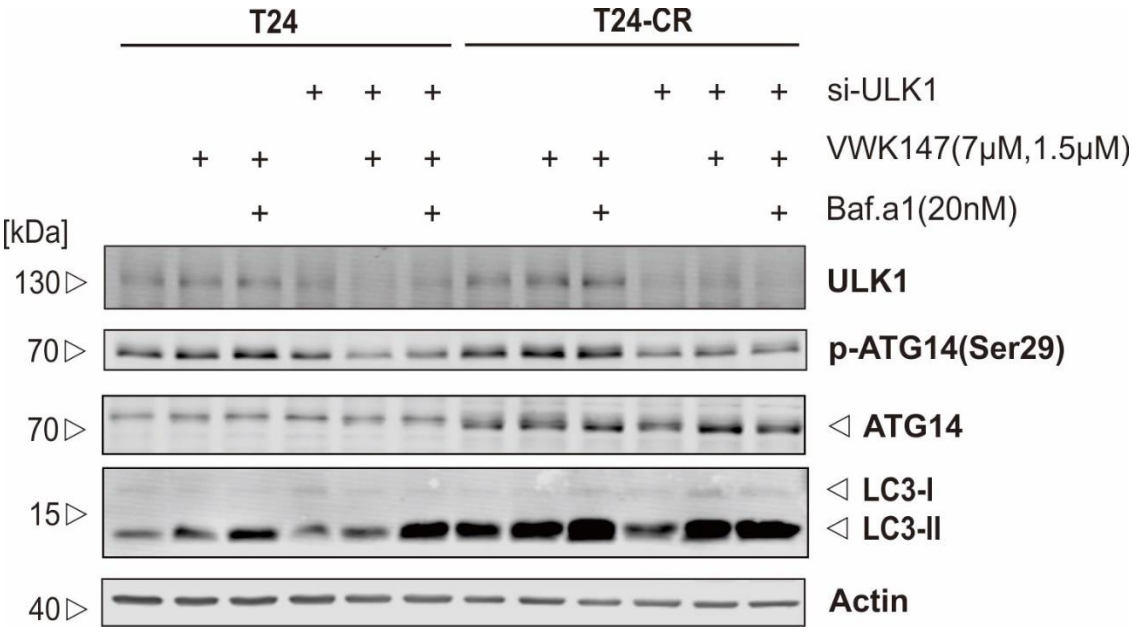

Figure 3.6.1: ULK1 knockdown does not affect VWK147-induced LC3 lipidation. T24 and T24-CR cells were transfected with siRNA against ULK1 or control siRNA for 48 hours. After transfection, cells were treated with VWK147 (7 μM, 1,5 μM respectively), with or without Baf.A1 (20 nM) for 24 hours. After incubation, cells were collected by scraping and lysed. 25 μg of total protein were loaded on the SDS-PAGE gels and analyzed by immunoblotting. Samples were analyzed for ULK1, pATG14 ser29, ATG14 and LC3. The housekeeping protein Actin was used as loading control.

We then employed *ulk1/2* DKO MEF cells to further confirm these results. After VWK147 treatment, *ulk1/2* DKO MEF cells had similar LC3-II levels as DKO cells reconstituted with ULK1 (figure 3.6.2). From these results, we can conclude that VWK147-induced LC3 lipidation was ULK1 independent, and is unlikely related to autophagy.

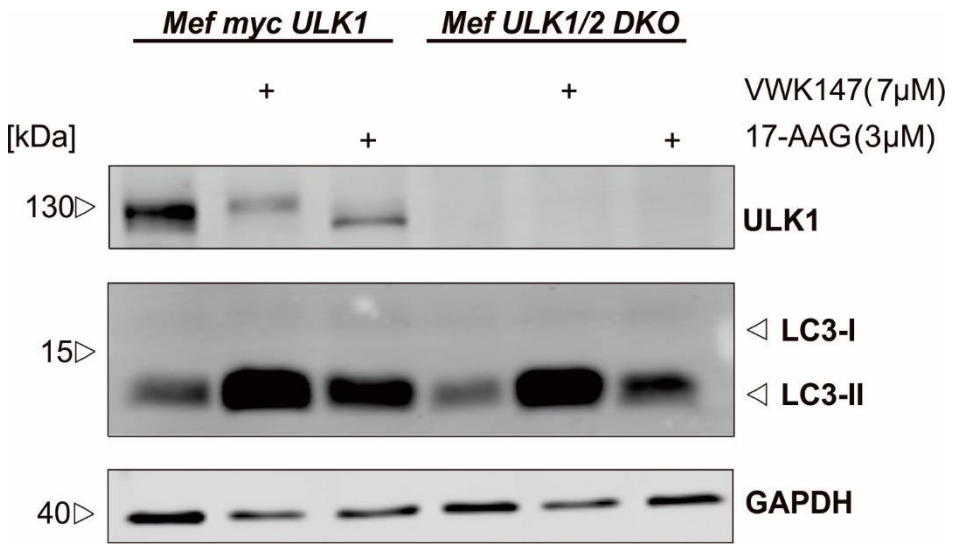

Figure 3.6.2: *ulk1/2* double knockout does not affect VWK147-induced LC3 lipidation. *ulk1/2* DKO and DKO MEFs reconstituted with myc-ULK1 were treated with VWK147 (7 μM) and 17-AAG (3 μM) for 24 hours. After incubation, cells were collected by scraping and lysed. 25 μg of total proteins were loaded on the SDS-PAGE gels and analyzed by immunoblotting. Samples were analyzed for ULK1, and LC3. The housekeeping protein GAPDH was used as loading control.

VPS34, also known as class III phosphatidylinositol 3-kinase, is located directly downstream of the ULK1 complex in the signaling network, and plays a major role in autophagy induction and autophagosome nucleation [85]. Therefore, it was explored whether PIK3C3 is involved in the lipidation of LC3 induced by VWK147. As shown in figure 3.6.3, SAR405, a potent and selective PI3KC3 inhibitor [86], inhibited autophagy in T24 and T24-CR cells, as can be deduced from a dose-dependent increase of P62, a classical autophagy receptor. As described in the introduction, PI3KC3 not only

participates in autophagosome generation but also in autophagosome trafficking. The inhibition of autophagosome trafficking may explain the increase in LC3-II level after the treatment of SAR405.

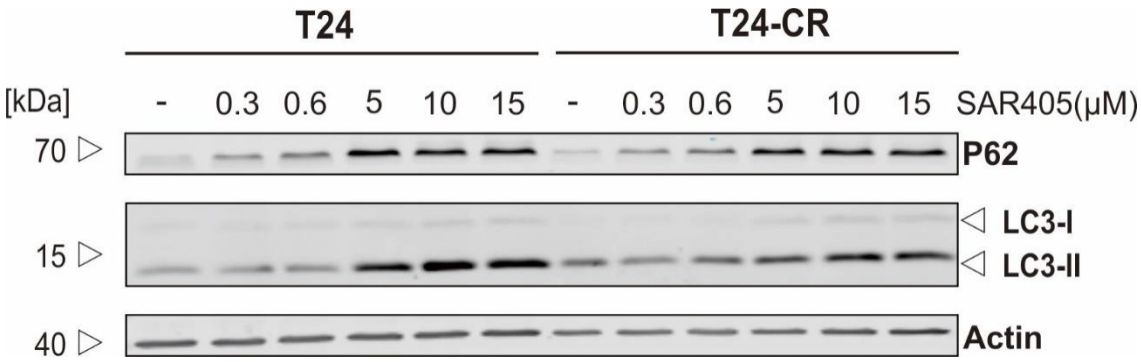

Figure 3.6.3: SAR405 inhibits autophagy in T24 and T24-CR cells. T24 and T24-CR cells were treated with different concentrations of SAR405 for 24 hours. After incubation, cells were collected by scraping and lysed. 25 µg of total proteins were loaded on the SDS-PAGE gels and analyzed by immunoblotting. Samples were analyzed for P62, and LC3. The housekeeping protein Actin was used as loading control.

To further explore if VWK147-induced LC3 lipidation was affected by PI3KC3, T24 and T24-CR cells were treated with VWK147 with or without SAR405. As shown in figure 3.6.4, VWK147-induced LC3 lipidation was not inhibited by SAR405, indicating that LC3 becomes lapidated independently of PI3KC3.

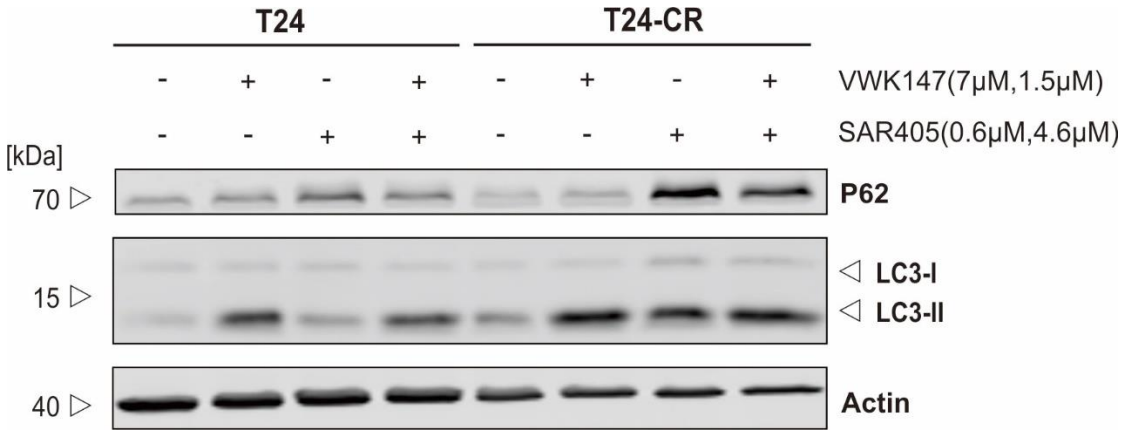

Figure 3.6.4: SAR405 does not inhibit VWK147-induced LC3 lipidation. T24 and T24-CR cells were treated with VWK147 (7 µM, 1.5 µM respectively), SAR405 (0.6 µM, 4.6 µM, i.e. approximate concentration of $IC_{50,}$ respectively [87]) or VWK147+SAR405 for 4 hours. After incubation, cells were collected by scraping and lysed. 25 µg of total proteins were loaded on the SDS-PAGE gels and analyzed by immunoblotting. Samples were analyzed for P62 and LC3. The housekeeping protein Actin was used as loading control.

The western blot results were further validated by immunofluorescence microscopy. The late endosome marker Rab7 is reported to participate in the final maturation of late autophagic vacuoles [88]. Here, the colocalization of Rab7 and LC3 puncta was used to indicate autophagosomes. As shown in figure 3.6.5, VWK147 can still increase $Rab7^{+}LC3^{+}$ dots when autophagy was blocked by SAR405. These results indicate that the lipidation of LC3 induced by VWK147 bypasses the requirement for PI3KC3. In summary, VWK147-induced non-canonical LC3 lipidation is ULK1- and PI3KC3-independent.

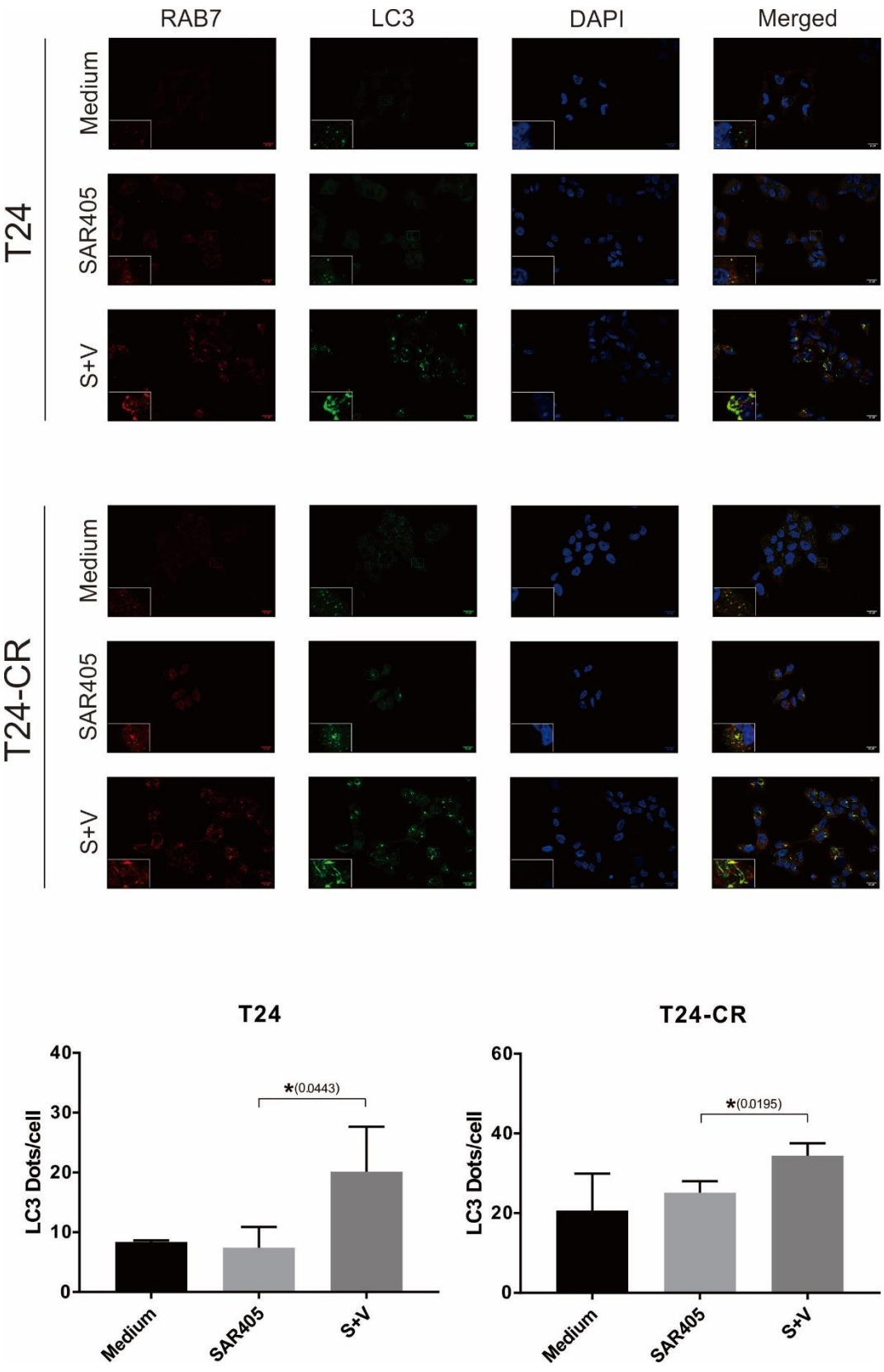

Figure 3.6.5: VWK147 induces RAB7 and LC3 double positive structures in T24 and T24-CR cells.

T24 and T24-CR cells were treated with SAR405 (0.6 μM and 4.6 μM) with or without VWK147 (7 μM

or 1.5 μM) for 6 hours. After the treatment, cells were fixed, permeabilized and immunostained for Rab7 and LC3. The Zeiss Axio Observer 7 fluorescence microscope (Zeiss, Köln, Germany) with a Plan Apochromat 40x/1.4 oil objective (Zeiss, Köln, Germany) was used for imaging. Nuclei were counterstained with DAPI. Scale bar: 20μm. Histograms showed the results of quantification analysis of the LC3 dots. The error bars represent the means + standard deviation (n=2).

4. Discussion

In this thesis, I report that both cisplatin-sensitive and -resistant bladder cancer cells show good response to of the inhibitors Torin2 and Hsp90. Of note, cisplatin-resistant cells are more sensitive to those treatments than their parental cells. Moreover, the N-terminal Hsp90 inhibitor 17-AAG and the C-terminal inhibitor VWK147 show different efficiency in terms of destabilization of client proteins. Notably, the combination of VWK147 and Torin2 are synergistic in both cisplatin -sensitive and -resistant cells, whereas combination of 17-AAG and Torin2 show synergistic effects only in T24 cells. Consequently, the combination treatment of VWK147 and Torin2 might be a promising cancer therapy, especially for cisplatin treatment failure cases.

Inhibitors for mTOR have been widely examined in various cancer models, including breast cancer, lung cancer, gastric carcinoma, prostate cancer, and bladder cancer, etc. However, the effects of mTOR inhibitors utilized as monotherapy in cancer are sometimes dampened by resistance mechanisms. Hence, it is logical that combined therapies with mTOR inhibitors and other pathway inhibitors or conventional therapies should be considered to improve treatment efficacy. Among the mechanisms of development of cellular resistance to mTOR inhibitors, a very important one is suppression of negative feedback loops, by which alternate proliferative signaling pathways are over-activated [81]. Among those over-activation pathways, many hub proteins are overexpressed or activated, such as MEK, IRS2, HER3 and AKT, etc. According to a list of Hsp90 client proteins provided by the Picard lab (https://www.picard.ch/downloads/Hsp90interactors.pdf), all these proteins are Hsp90 client proteins. Therefore, combining mTOR inhibitors with Hsp90 inhibitors would be promising to improve treatment effects in cancers. The combination of these two is worth for further research in different cancer models.

In the past few years, the N-terminal Hsp90 inhibitors have been researched as an

attractive strategy for anti-cancer therapy. But despite many efforts in this field, none of them have been currently involved in clinical trials because the detrimental HSR has been shown to be induced. Therefore, the C-terminal Hsp90 inhibitors have become a more promising alternative strategy for anti-cancer treatment without triggering this cell rescue cascade. Theoretically, the C-terminal Hsp90 inhibitors should be more prominent in destabilizing client proteins compared to N-terminal Hsp90 inhibitors. However, in this work, the N-terminal Hsp90 inhibitor 17-AAG more prominently reduced the abundance of clients C-RAP, RIPK1, AKT and ULK1. Therefore, it is valuable to test the Hsp90 binding efficiency of VWK147 and off-target effects of VWK147. Besides, more Hsp90 client proteins should be tested under 17-AAG and VWK147 treatment to see if there are differences between them. These clients might help to explain the synergistic combination effects between VWK147 and Torin2. In addition, this work also shows that the cisplatin resistant bladder cancer cells are more sensitive to Hsp90 inhibitors than its parental cells. It would also be interesting to investigate the reasons for that. The different sensitivity to Hsp90 inhibitors might offer an opening window to cope with cisplatin resistant bladder cancer.

The lipidation of ATG8, a family of ubiquitin-like proteins including LC3A/B/B2/C and GABARAP/L1/L2, is a defining feature of autophagy. ATG8 can be conjugated to PE or PS [89]. After cleavage of the nascent pro-ATG8 mostly by the cysteine protease ATG4, a C-terminal conserved aromatic-Gly motif is exposed. The nonlipidated and lipidated forms are usually referred to as LC3-I and LC3-II, or GABARAP and GABARAP-PE. During autophagy, autophagosomes fuse with lysosomes, leading to the proteolytic degradation of LC3-II located to inner membranes of autophagosomes. In addition, Tanida et al reported that hATG4B delipidates endogenous LC3-II and GABARAP-II in vitro [90]. Therefore, the protease activity of ATG4 and proteolytic activity of lysosomes are highly related to LC3 lipidation level. In this work, LC3-II protein abundance was found to increase after VWK147 treatment. It will be interesting to test if VWK147 treatment disturbs proteolytic activity of lysosomes, since partial

inhibition of lysosomes can also increase the abundance of LC3-II, even though VWK147 induces the synthesis of autophagosomes (see figure 3.5.3). Besides, it is also valuable to know if VWK147 affects protease activity of ATG4 or if Hsp90 is involved in the process of ATG4-mediated delipidation of LC3-II. According to the supplementary figure 6.2.2, VWK147 induced LAMP-1 and LC3 accumulation, but their colocalization was not found. These results suggest VWK147-induced LC3 accumulation might be non-canonical autophagy or LC3 lipidation, which might execute autophagy-independent function(s). So far, it has been reported that LC3 has a variety of non-autophagy effects, such as interaction with GTPases, ATG8-GAP interaction as a regulatory signal platform, and regulation of GEF (guanine-nucleotide exchange factor) activity [91]. Of interest, among the non-autophagic roles of LC3, non-lipidated ATG8/LC3 (LC3-I) executes distinct roles, such as being a regulator of coronaviruses replication [92] or a regulator of yeast vacuole fusion [93].

There is much knowledge about the targeting of ATG8 lipidation in autophagy, but little is known about how this response is targeted in autophagy-independent events. Recently, non-canonical autophagy, including single-membrane and double-membrane structures, has been found in various conditions. So far, it is believed that non-canonical autophagy pathways and structures have the same functions as canonical autophagy in isolating some of the cytoplasm and separating pathogens. In many cases, substrates sequestered by non-canonical autophagy will eventually be degraded in the lysosomal compartment [94]. However, there are two important questions that require further research. The first question is whether non-canonical autophagy has specific functions in cell physiology or in pathological situations. The second question aims at the relationship between non-canonical autophagy and selective autophagy such as xenophagy and mitophagy. In this work, only VWK147 was found to induce non-canonical LC3 lipidation, not the N-terminal Hsp90 inhibitor 17-AAG. Similarly, only VWK147 had synergistic effects with Torin2 in cisplatin-resistant bladder cancer cells. Whether these two phenomena are coincident or related needs to be clarified in the future.

In summary, this work shows that the combination of Torin2 and two Hsp90 inhibitors is synergistic in different BC cell lines. Moreover, the C-terminal inhibitor VWK147 acts synergistically with Torin2 in cisplatin resistant BCs, whereas 17-AAG shows additive or even rather antagonistic effects. This study provides evidence of this promising combination therapy for patients with bladder cancer.

5. References

1. Ferlay J, Colombet M, Soerjomataram I, Dyba T, Randi G, Bettio M, et al. Cancer incidence and mortality patterns in Europe: Estimates for 40 countries and 25 major cancers in 2018. European journal of cancer (Oxford, England : 1990). 2018;103:356–87. doi:10.1016/j.ejca.2018.07.005.
2. Burger M, Catto JWF, Dalbagni G, Grossman HB, Herr H, Karakiewicz P, et al. Epidemiology and risk factors of urothelial bladder cancer. European Urology. 2013;63:234–41. doi:10.1016/j.eururo.2012.07.033.
3. Smith AB, Deal AM, Woods ME, Wallen EM, Pruthi RS, Chen RC, et al. Muscle-invasive bladder cancer: evaluating treatment and survival in the National Cancer Data Base. BJU International. 2014;114:719–26. doi:10.1111/bju.12601.
4. Chen GK, Durán GE, Mangili A, Beketic-Oreskovic L, Sikic BI. MDR 1 activation is the predominant resistance mechanism selected by vinblastine in MES-SA cells. British journal of cancer. 2000;83:892–8. doi:10.1054/bjoc.2000.1371.
5. Grossman HB, Natale RB, Tangen CM, Speights VO, Vogelzang NJ, Trump DL, et al. Neoadjuvant chemotherapy plus cystectomy compared with cystectomy alone for locally advanced bladder cancer. The New England journal of medicine. 2003;349:859–66. doi:10.1056/NEJMoa022148.
6. Marina N, Chang KW, Malogolowkin M, London WB, Frazier AL, Womer RB, et al. Amifostine does not protect against the ototoxicity of high-dose cisplatin combined with etoposide and bleomycin in pediatric germ-cell tumors: a Children's Oncology Group study. Cancer. 2005;104:841–7. doi:10.1002/cncr.21218.
7. Babjuk M, Burger M, Zigeuner R, Shariat SF, van Rhijn BWG, Compérat E, et al. EAU guidelines on non-muscle-invasive urothelial carcinoma of the bladder: update 2013. European Urology. 2013;64:639–53. doi:10.1016/j.eururo.2013.06.003.
8. Choi W, Porten S, Kim S, Willis D, Plimack ER, Hoffman-Censits J, et al. Identification of distinct basal and luminal subtypes of muscle-invasive bladder cancer with different sensitivities to frontline chemotherapy. Cancer cell. 2014;25:152–65. doi:10.1016/j.ccr.2014.01.009.
9. Lindgren D, Frigyesi A, Gudjonsson S, Sjödahl G, Hallden C, Chebil G, et al. Combined gene expression and genomic profiling define two intrinsic molecular subtypes of urothelial carcinoma and gene signatures for molecular grading and outcome. Cancer Res. 2010:3463–72. doi:10.1158/0008-5472.CAN-09-4213.
10. Robertson AG, Kim J, Al-Ahmadie H, Bellmunt J, Guo G, Cherniack AD, et al. Comprehensive Molecular Characterization of Muscle-Invasive Bladder Cancer. Cell. 2017:540-556.e25. doi:10.1016/j.cell.2017.09.007.
11. Hedegaard J, Lamy P, Nordentoft I, Algaba F, Høyer S, Ulhøi BP, et al. Comprehensive Transcriptional Analysis of Early-Stage Urothelial Carcinoma. Cancer cell. 2016;30:27–42. doi:10.1016/j.ccell.2016.05.004.
12. Tran L, Xiao J-F, Agarwal N, Duex JE, Theodorescu D. Advances in bladder cancer biology and therapy. Nature reviews. Cancer 2020. doi:10.1038/s41568-020-00313-1.

13. Loehrer PJ, Einhorn LH, Elson PJ, Crawford ED, Kuebler P, Tannock I, et al. A randomized comparison of cisplatin alone or in combination with methotrexate, vinblastine, and doxorubicin in patients with metastatic urothelial carcinoma: a cooperative group study. Journal of clinical oncology : official journal of the American Society of Clinical Oncology. 1992;10:1066–73. doi:10.1200/JCO.1992.10.7.1066.
14. Stein JP, Lieskovsky G, Cote R, Groshen S, Feng AC, Boyd S, et al. Radical cystectomy in the treatment of invasive bladder cancer: long-term results in 1,054 patients. Journal of clinical oncology : official journal of the American Society of Clinical Oncology. 2001;19:666–75. doi:10.1200/JCO.2001.19.3.666.
15. NIH. Cancer stat facts: bladder cancer. National Cancer Institute Surveillance, Epidemiology and End Results Program. 2017.
16. Köberle B, Tomicic MT, Usanova S, Kaina B. Cisplatin resistance: preclinical findings and clinical implications. Biochimica et biophysica acta. 2010;1806:172–82. doi:10.1016/j.bbcan.2010.07.004.
17. Kelland L. The resurgence of platinum-based cancer chemotherapy. Nature reviews. Cancer. 2007;7:573–84. doi:10.1038/nrc2167.
18. Ma KL, Liu J, Gao M, Wang CX, Ni J, Zhang Y, et al. Activation of mTOR contributes to foam cell formation in the radial arteries of patients with end-stage renal disease. Clinical nephrology. 2014;81:396–404. doi:10.5414/CN108189.
19. Saxton RA, Sabatini DM. mTOR Signaling in Growth, Metabolism, and Disease. Cell. 2017;168:960–76. doi:10.1016/j.cell.2017.02.004.
20. Zoncu R, Efeyan A, Sabatini DM. mTOR: from growth signal integration to cancer, diabetes and ageing. Nature reviews. Molecular cell biology. 2011;12:21–35. doi:10.1038/nrm3025.
21. Alers S, Löffler AS, Wesselborg S, Stork B. Role of AMPK-mTOR-Ulk1/2 in the regulation of autophagy: cross talk, shortcuts, and feedbacks. Mol Cell Biol. 2012:2–11. doi:10.1128/MCB.06159-11.
22. Comprehensive molecular characterization of urothelial bladder carcinoma. Nature. 2014;507:315–22. doi:10.1038/nature12965.
23. Chiong E, Lee I-L, Dadbin A, Sabichi AL, Harris L, Urbauer D, et al. Effects of mTOR inhibitor everolimus (RAD001) on bladder cancer cells. Clin Cancer Res. 2011;17:2863–73. doi:10.1158/1078-0432.CCR-09-3202.
24. Guo Y, Chekaluk Y, Zhang J, Du J, Gray NS, Wu C-L, Kwiatkowski DJ. TSC1 involvement in bladder cancer: diverse effects and therapeutic implications. The Journal of Pathology. 2013;230:17–27. doi:10.1002/path.4176.
25. Kang SA, Pacold ME, Cervantes CL, Lim D, Lou HJ, Ottina K, et al. mTORC1 phosphorylation sites encode their sensitivity to starvation and rapamycin. Science. 2013;341:1236566. doi:10.1126/science.1236566.
26. Tabernero J, Rojo F, Calvo E, Burris H, Judson I, Hazell K, et al. Dose- and schedule-dependent inhibition of the mammalian target of rapamycin pathway with everolimus: a phase I tumor pharmacodynamic study in patients with advanced solid tumors. Journal of clinical oncology : official journal of the American Society of Clinical Oncology. 2008:1603–10. doi:10.1200/JCO.2007.14.5482.

27. Palm W, Park Y, Wright K, Pavlova NN, Tuveson DA, Thompson CB. The Utilization of Extracellular Proteins as Nutrients Is Suppressed by mTORC1. Cell. 2015;162:259–70. doi:10.1016/j.cell.2015.06.017.
28. Liu Q, Xu C, Kirubakaran S, Zhang X, Hur W, Liu Y, et al. Characterization of Torin2, an ATP-competitive inhibitor of mTOR, ATM, and ATR. Cancer Res. 2013;73:2574–86. doi:10.1158/0008-5472.CAN-12-1702.
29. Pearl LH, Prodromou C. Structure and mechanism of the Hsp90 molecular chaperone machinery. Annual review of biochemistry. 2006;75:271–94. doi:10.1146/annurev.biochem.75.103004.142738.
30. Miyata Y, Nakamoto H, Neckers L. The therapeutic target Hsp90 and cancer hallmarks. Current pharmaceutical design. 2013;19:347–65. doi:10.2174/138161213804143725.
31. Koren J, Blagg BSJ. The Right Tool for the Job: An Overview of Hsp90 Inhibitors. Adv Exp Med Biol. 2020;1243:135–46. doi:10.1007/978-3-030-40204-4_9.
32. Prodromou C, Pearl LH. Structure and functional relationships of Hsp90. Current cancer drug targets. 2003;3:301–23. doi:10.2174/1568009033481877.
33. Krukenberg KA, Street TO, Lavery LA, Agard DA. Conformational dynamics of the molecular chaperone Hsp90. Q Rev Biophys. 2011;44:229–55. doi:10.1017/S0033583510000314.
34. Sauvage F, Messaoudi S, Fattal E, Barratt G, Vergnaud-Gauduchon J. Heat shock proteins and cancer: How can nanomedicine be harnessed? Journal of controlled release : official journal of the Controlled Release Society. 2017;248:133–43. doi:10.1016/j.jconrel.2017.01.013.
35. Barrott JJ, Haystead TAJ. Hsp90, an unlikely ally in the war on cancer. FEBS J. 2013;280:1381–96. doi:10.1111/febs.12147.
36. Pearl LH, Prodromou C. Structure and mechanism of the Hsp90 molecular chaperone machinery. Annual review of biochemistry. 2006;75:271–94. doi:10.1146/annurev.biochem.75.103004.142738.
37. Reed SI. The selection of S. cerevisiae mutants defective in the start event of cell division. Genetics. 1980;95:561–77.
38. Taipale M, Krykbaeva I, Koeva M, Kayatekin C, Westover KD, Karras GI, Lindquist S. Quantitative analysis of HSP90-client interactions reveals principles of substrate recognition. Cell. 2012;150:987–1001. doi:10.1016/j.cell.2012.06.047.
39. Lu X, Xiao L, Wang L, Ruden DM. Hsp90 inhibitors and drug resistance in cancer: the potential benefits of combination therapies of Hsp90 inhibitors and other anti-cancer drugs. Biochem Pharmacol. 2012;83:995–1004. doi:10.1016/j.bcp.2011.11.011.
40. Sanli O, Dobruch J, Knowles MA, Burger M, Alemozaffar M, Nielsen ME, Lotan Y. Bladder cancer. Nat Rev Dis Primers. 2017;3:17022. doi:10.1038/nrdp.2017.22.
41. Lu X, Xiao L, Wang L, Ruden DM. Hsp90 inhibitors and drug resistance in cancer: the potential benefits of combination therapies of Hsp90 inhibitors and other anti-cancer drugs. Biochem Pharmacol. 2012;83:995–1004. doi:10.1016/j.bcp.2011.11.011.
42. Jonkers J, Berns A. Oncogene addiction: sometimes a temporary slavery. Cancer

cell. 2004;6:535–8. doi:10.1016/j.ccr.2004.12.002.
43. Kamal A, Thao L, Sensintaffar J, Zhang L, Boehm MF, Fritz LC, Burrows FJ. A high-affinity conformation of Hsp90 confers tumour selectivity on Hsp90 inhibitors. Nature. 2003;425:407–10. doi:10.1038/nature01913.
44. Chandran T, Katragadda U, Teng Q, Tan C. Design and evaluation of micellar nanocarriers for 17-allyamino-17-demethoxygeldanamycin (17-AAG). Int J Pharm. 2010:170–7. doi:10.1016/j.ijpharm.2010.03.056.
45. Onyüksel H, Mohanty PS, Rubinstein I. VIP-grafted sterically stabilized phospholipid nanomicellar 17-allylamino-17-demethoxy geldanamycin: a novel targeted nanomedicine for breast cancer. Int J Pharm. 2009:157–61. doi:10.1016/j.ijpharm.2008.08.024.
46. Bagatell R, Paine-Murrieta GD, Taylor CW, Pulcini EJ, Akinaga S, Benjamin IJ, Whitesell L. Induction of a heat shock factor 1-dependent stress response alters the cytotoxic activity of hsp90-binding agents. Clin Cancer Res. 2000;6:3312–8.
47. Maloney A, Clarke PA, Naaby-Hansen S, Stein R, Koopman J-O, Akpan A, et al. Gene and protein expression profiling of human ovarian cancer cells treated with the heat shock protein 90 inhibitor 17-allylamino-17-demethoxygeldanamycin. Cancer research. 2007;67:3239–53. doi:10.1158/0008-5472.CAN-06-2968.
48. Butler LM, Ferraldeschi R, Armstrong HK, Centenera MM, Workman P. Maximizing the Therapeutic Potential of HSP90 Inhibitors. Molecular cancer research : MCR. 2015;13:1445–51. doi:10.1158/1541-7786.MCR-15-0234.
49. McCollum AK, Teneyck CJ, Sauer BM, Toft DO, Erlichman C. Up-regulation of heat shock protein 27 induces resistance to 17-allylamino-demethoxygeldanamycin through a glutathione-mediated mechanism. Cancer research. 2006;66:10967–75. doi:10.1158/0008-5472.CAN-06-1629.
50. Klionsky DJ. Autophagy revisited: a conversation with Christian de Duve. Autophagy. 2008:740–3. doi:10.4161/auto.6398.
51. Ravanan P, Srikumar IF, Talwar P. Autophagy: The spotlight for cellular stress responses. Life Sci. 2017:53–67. doi:10.1016/j.lfs.2017.08.029.
52. Galluzzi L, Vitale I, Aaronson SA, Abrams JM, Adam D, Agostinis P, et al. Molecular mechanisms of cell death: recommendations of the Nomenclature Committee on Cell Death 2018. Cell Death Differ. 2018:486–541. doi:10.1038/s41418-017-0012-4.
53. Kaushik S, Cuervo AM. The coming of age of chaperone-mediated autophagy. Nature reviews. Molecular cell biology. 2018;19:365–81. doi:10.1038/s41580-018-0001-6.
54. Schuck S. Microautophagy - distinct molecular mechanisms handle cargoes of many sizes. J Cell Sci 2020. doi:10.1242/jcs.246322.
55. Yu L, Chen Y, Tooze SA. Autophagy pathway: Cellular and molecular mechanisms. Autophagy. 2018:207–15. doi:10.1080/15548627.2017.1378838.
56. Stork B, Dengjel J. Study of ULK1 Catalytic Activity and Its Regulation. Methods in enzymology. 2017;587:391–404. doi:10.1016/bs.mie.2016.09.067.
57. Nishimura T, Mizushima N. The ULK complex initiates autophagosome formation at phosphatidylinositol synthase-enriched ER subdomains. Autophagy. 2017:1795–

6. doi:10.1080/15548627.2017.1358344.
58. Sun Q, Fan W, Zhong Q. Regulation of Beclin 1 in autophagy. Autophagy. 2009:713–6. doi:10.4161/auto.5.5.8524.
59. Yamashita S-I, Kanki T. How autophagy eats large mitochondria: Autophagosome formation coupled with mitochondrial fragmentation. Autophagy. 2017;13:980–1. doi:10.1080/15548627.2017.1291113.
60. Proikas-Cezanne T, Takacs Z, Dönnes P, Kohlbacher O. WIPI proteins: essential PtdIns3P effectors at the nascent autophagosome. J Cell Sci. 2015;128:207–17. doi:10.1242/jcs.146258.
61. Mizushima N. The ATG conjugation systems in autophagy. Curr Opin Cell Biol. 2020:1–10. doi:10.1016/j.ceb.2019.12.001.
62. Wang Y, Li L, Hou C, Lai Y, Long J, Liu J, et al. SNARE-mediated membrane fusion in autophagy. Semin Cell Dev Biol. 2016:97–104. doi:10.1016/j.semcdb.2016.07.009.
63. Levy JMM, Towers CG, Thorburn A. Targeting autophagy in cancer. Nature reviews. Cancer. 2017:528–42. doi:10.1038/nrc.2017.53.
64. Amaravadi R, Kimmelman AC, White E. Recent insights into the function of autophagy in cancer. Genes Dev. 2016;30:1913–30. doi:10.1101/gad.287524.116.
65. White E. Deconvoluting the context-dependent role for autophagy in cancer. Nature reviews. Cancer. 2012;12:401–10. doi:10.1038/nrc3262.
66. Chi K-H, Ko H-L, Yang K-L, Lee C-Y, Chi M-S, Kao S-J. Addition of rapamycin and hydroxychloroquine to metronomic chemotherapy as a second line treatment results in high salvage rates for refractory metastatic solid tumors: a pilot safety and effectiveness analysis in a small patient cohort. Oncotarget. 2015;6:16735–45. doi:10.18632/oncotarget.3793.
67. Mahalingam D, Mita M, Sarantopoulos J, Wood L, Amaravadi RK, Davis LE, et al. Combined autophagy and HDAC inhibition: a phase I safety, tolerability, pharmacokinetic, and pharmacodynamic analysis of hydroxychloroquine in combination with the HDAC inhibitor vorinostat in patients with advanced solid tumors. Autophagy. 2014;10:1403–14. doi:10.4161/auto.29231.
68. Akin D, Wang SK, Habibzadegah-Tari P, Law B, Ostrov D, Li M, et al. A novel ATG4B antagonist inhibits autophagy and has a negative impact on osteosarcoma tumors. Autophagy. 2014:2021–35. doi:10.4161/auto.32229.
69. Dowdle WE, Nyfeler B, Nagel J, Elling RA, Liu S, Triantafellow E, et al. Selective VPS34 inhibitor blocks autophagy and uncovers a role for NCOA4 in ferritin degradation and iron homeostasis in vivo. Nat Cell Biol. 2014;16:1069–79. doi:10.1038/ncb3053.
70. Petherick KJ, Conway OJL, Mpamhanga C, Osborne SA, Kamal A, Saxty B, Ganley IG. Pharmacological inhibition of ULK1 kinase blocks mammalian target of rapamycin (mTOR)-dependent autophagy. J Biol Chem. 2015:11376–83. doi:10.1074/jbc.C114.627778.
71. Liu ST, Hui G, Mathis C, Chamie K, Pantuck AJ, Drakaki A. The Current Status and Future Role of the Phosphoinositide 3 Kinase/AKT Signaling Pathway in Urothelial Cancer: An Old Pathway in the New Immunotherapy Era. Clin

Genitourin Cancer. 2018;16:e269-e276. doi:10.1016/j.clgc.2017.10.011.
72. Kim J, Kundu M, Viollet B, Guan K-L. AMPK and mTOR regulate autophagy through direct phosphorylation of Ulk1. Nat Cell Biol. 2011;13:132–41. doi:10.1038/ncb2152.
73. Schopf FH, Biebl MM, Buchner J. The HSP90 chaperone machinery. Nature reviews. Molecular cell biology. 2017;18:345–60. doi:10.1038/nrm.2017.20.
74. Tatokoro M, Koga F, Yoshida S, Kawakami S, Fujii Y, Neckers L, Kihara K. Potential role of Hsp90 inhibitors in overcoming cisplatin resistance of bladder cancer-initiating cells. Int J Cancer. 2012;131:987–96. doi:10.1002/ijc.26475.
75. Modi S, Stopeck AT, Gordon MS, Mendelson D, Solit DB, Bagatell R, et al. Combination of trastuzumab and tanespimycin (17-AAG, KOS-953) is safe and active in trastuzumab-refractory HER-2 overexpressing breast cancer: a phase I dose-escalation study. Journal of clinical oncology : official journal of the American Society of Clinical Oncology. 2007;25:5410–7. doi:10.1200/JCO.2007.11.7960.
76. Pacey S, Banerji U, Judson I, Workman P. Hsp90 inhibitors in the clinic. Handb Exp Pharmacol. 2006:331–58. doi:10.1007/3-540-29717-0_14.
77. Kijima T, Prince TL, Tigue ML, Yim KH, Schwartz H, Beebe K, et al. HSP90 inhibitors disrupt a transient HSP90-HSF1 interaction and identify a noncanonical model of HSP90-mediated HSF1 regulation. Sci Rep. 2018;8:6976. doi:10.1038/s41598-018-25404-w.
78. Li Y, Zhang T, Schwartz SJ, Sun D. New developments in Hsp90 inhibitors as anti-cancer therapeutics: mechanisms, clinical perspective and more potential. Drug Resist Updat. 2009;12:17–27. doi:10.1016/j.drup.2008.12.002.
79. Wang Y, McAlpine SR. Heat-shock protein 90 inhibitors: will they ever succeed as chemotherapeutics? Future Med Chem. 2015;7:87–90. doi:10.4155/fmc.14.154.
80. Hua H, Kong Q, Zhang H, Wang J, Luo T, Jiang Y. Targeting mTOR for cancer therapy. J Hematol Oncol. 2019;12:71. doi:10.1186/s13045-019-0754-1.
81. Faes S, Demartines N, Dormond O. Resistance to mTORC1 Inhibitors in Cancer Therapy: From Kinase Mutations to Intratumoral Heterogeneity of Kinase Activity. Oxid Med Cell Longev. 2017;2017:1726078. doi:10.1155/2017/1726078.
82. Chou T-C. Drug combination studies and their synergy quantification using the Chou-Talalay method. Cancer Res. 2010;70:440–6. doi:10.1158/0008-5472.CAN-09-1947.
83. Behrends C, Sowa ME, Gygi SP, Harper JW. Network organization of the human autophagy system. Nature. 2010;466:68–76. doi:10.1038/nature09204.
84. Zhou C, Qian X, Hu M, Zhang R, Liu N, Huang Y, et al. STYK1 promotes autophagy through enhancing the assembly of autophagy-specific class III phosphatidylinositol 3-kinase complex I. Autophagy. 2019:1–21. doi:10.1080/15548627.2019.1687212.
85. Wirth M, Joachim J, Tooze SA. Autophagosome formation--the role of ULK1 and Beclin1-PI3KC3 complexes in setting the stage. Seminars in cancer biology. 2013;23:301–9. doi:10.1016/j.semcancer.2013.05.007.
86. Ronan B, Flamand O, Vescovi L, Dureuil C, Durand L, Fassy F, et al. A highly potent and selective Vps34 inhibitor alters vesicle trafficking and autophagy. Nat

Chem Biol. 2014;10:1013–9. doi:10.1038/nchembio.1681.
87. Schlütermann D, Skowron MA, Berleth N, Böhler P, Deitersen J, Stuhldreier F, et al. Targeting urothelial carcinoma cells by combining cisplatin with a specific inhibitor of the autophagy-inducing class III PtdIns3K complex. Urol Oncol. 2018;36:160.e1-160.e13. doi:10.1016/j.urolonc.2017.11.021.
88. Gutierrez MG, Munafó DB, Berón W, Colombo MI. Rab7 is required for the normal progression of the autophagic pathway in mammalian cells. J Cell Sci. 2004;117:2687–97. doi:10.1242/jcs.01114.
89. Durgan J, Lystad AH, Sloan K, Carlsson SR, Wilson MI, Marcassa E, et al. Non-canonical autophagy drives alternative ATG8 conjugation to phosphatidylserine. Molecular Cell. 2021;81:2031-2040.e8. doi:10.1016/j.molcel.2021.03.020.
90. Tanida I, Ueno T, Kominami E. LC3 conjugation system in mammalian autophagy. Int J Biochem Cell Biol. 2004;36:2503–18. doi:10.1016/j.biocel.2004.05.009.
91. Subramani S, Malhotra V. Non-autophagic roles of autophagy-related proteins. EMBO Rep. 2013;14:143–51. doi:10.1038/embor.2012.220.
92. Reggiori F, Monastyrska I, Verheije MH, Calì T, Ulasli M, Bianchi S, et al. Coronaviruses Hijack the LC3-I-positive EDEMosomes, ER-derived vesicles exporting short-lived ERAD regulators, for replication. Cell Host Microbe. 2010;7:500–8. doi:10.1016/j.chom.2010.05.013.
93. Tamura N, Oku M, Sakai Y. Atg8 regulates vacuolar membrane dynamics in a lipidation-independent manner in Pichia pastoris. J Cell Sci. 2010;123:4107–16. doi:10.1242/jcs.070045.
94. Codogno P, Mehrpour M, Proikas-Cezanne T. Canonical and non-canonical autophagy: variations on a common theme of self-eating? Nat Rev Mol Cell Biol. 2012;13:7–12. doi:10.1038/nrm3249.

6. Appendix

6.1 List of figures

6.2 Supplementary figures

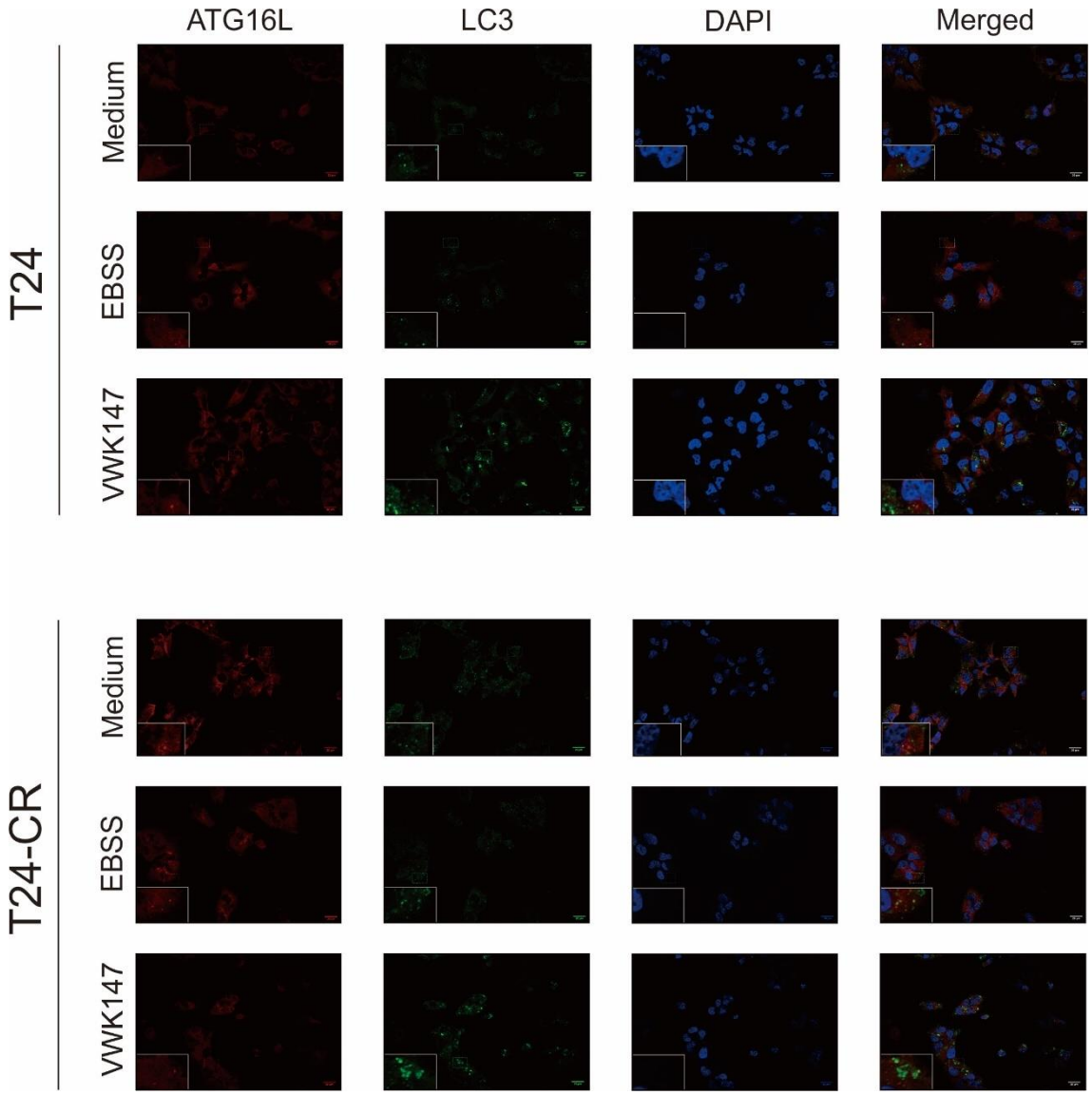

Figure 6.2.1: VWK147 does not induces ATG16L puncta formation in T24 and T24-CR cells. T24 and T24-CR cells were treated with VWK147 (7 µM and 1.5 µM) for 6 hours or with EBSS for 2 hours. After the treatment, cells were fixed, permeabilized and immunostained for ATG16L and LC3. Imaging was performed using an inverse confocal laser scanning microscope. Nuclei were counterstained with DAPI. Scale bar: 20µm.

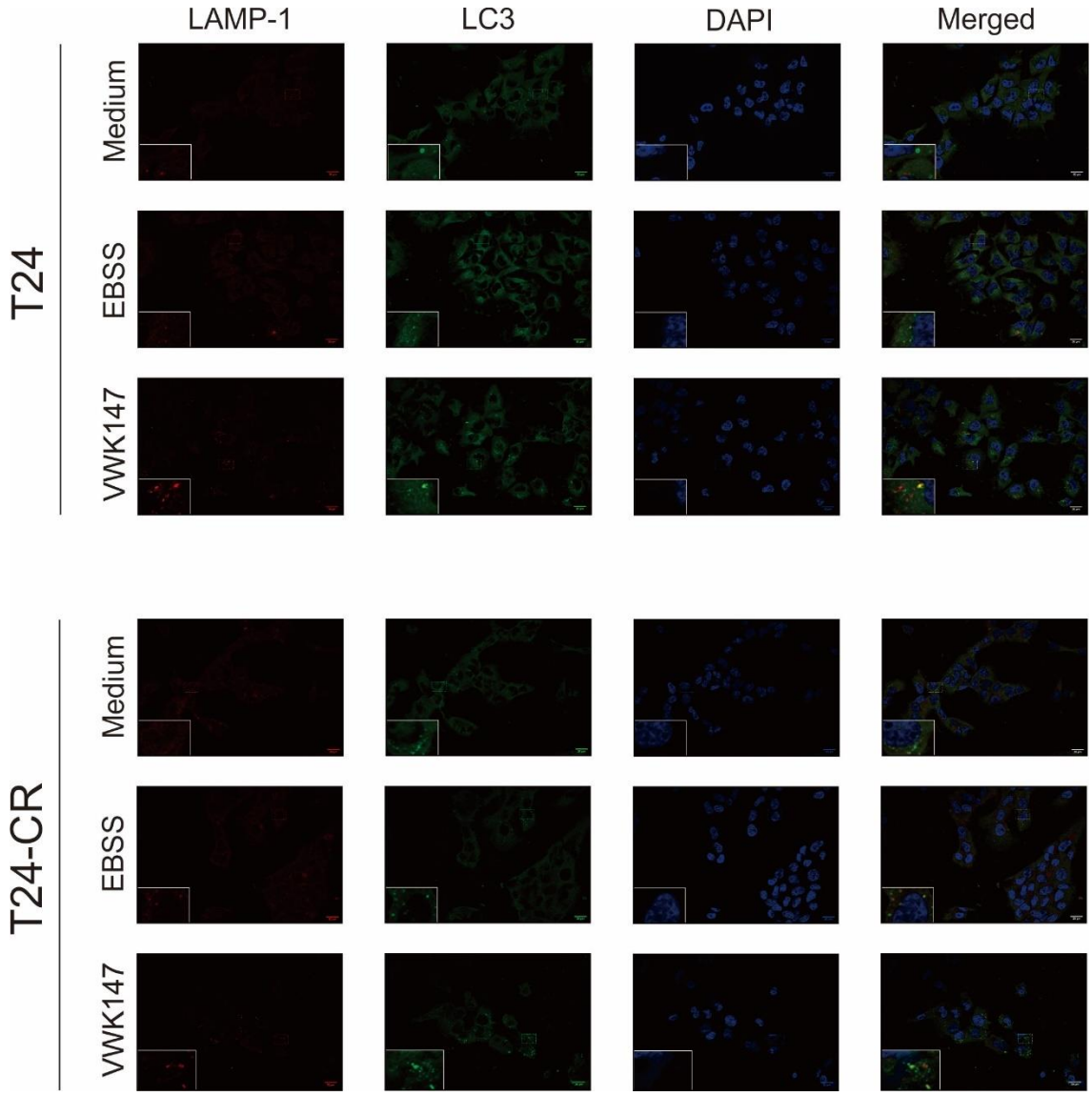

Figure 6.2.2: VWK147 does not induces LAMP-1 puncta formation in T24 and T24-CR cells. T24 and T24-CR cells were treated with VWK147 (7 μM and 1.5 μM) for 6 hours or with EBSS for 2 hours. After the treatment, cells were fixed, permeabilized and immunostained for LAMP-1 and LC3. The Zeiss Axio Observer 7 fluorescence microscope (Zeiss, Köln, Germany) with a Plan Apochromat 40x/1.4 oil objective (Zeiss, Köln, Germany) was used for imaging. Nuclei were counterstained with DAPI. Scale bar: 20μm.

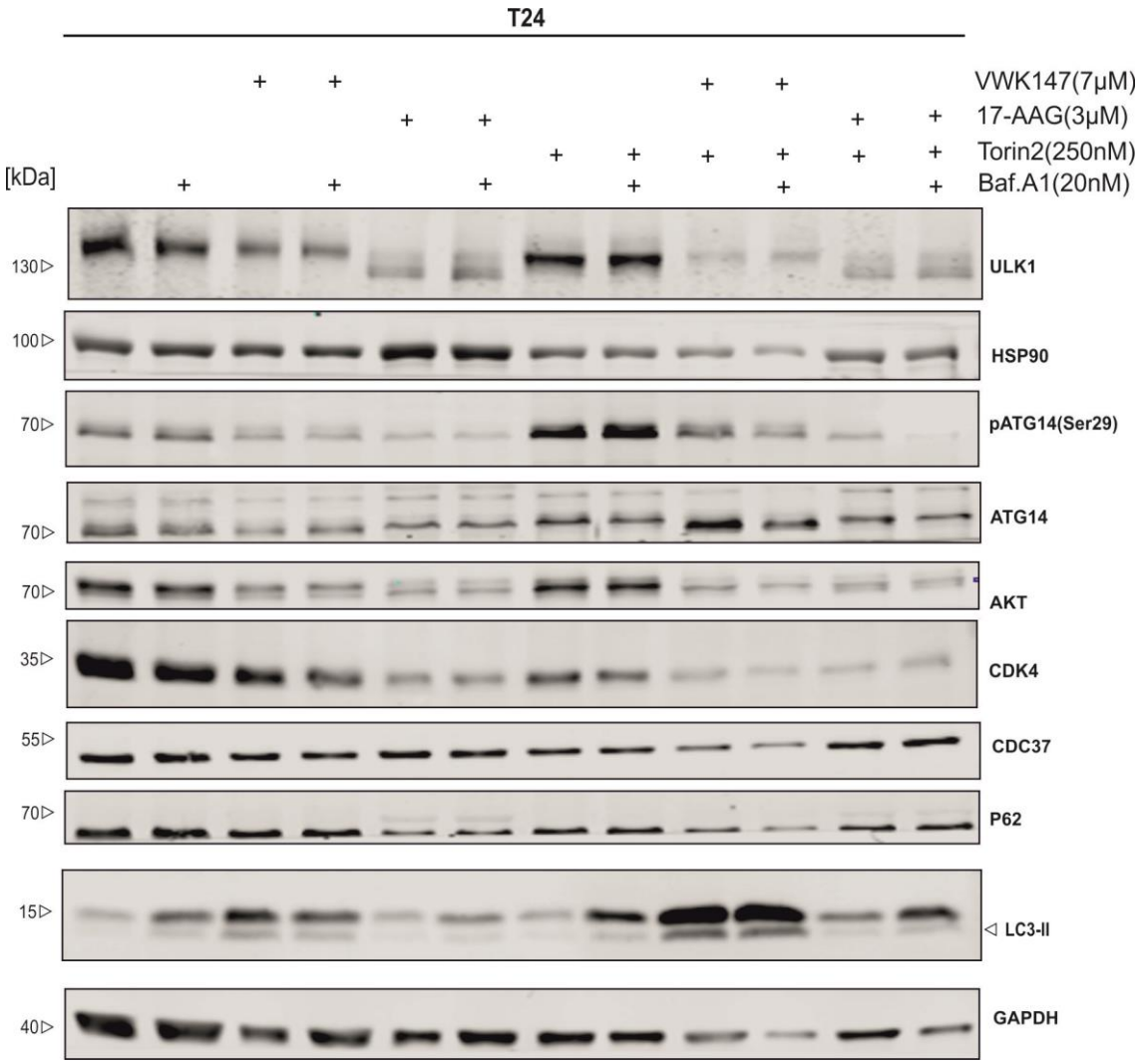

Figure 6.2.3: Immunoblotting results of Hsp90 clients and autophagy markers in T24 cells. T24 cells were treated with VWK147 (7 µM), 17-AAG (3 µM), Torin2 (250 nM), and Baf.A1 (20 nM) separately or in combination for 24 hours. After incubation, cells were collected by scraping and lysed. 25 µg of total protein were loaded on the SDS-PAGE gels and analyzed by immunoblotting. Samples were analyzed for ULK1, Hsp90, pATG14 ser29, ATG14, AKT, CDK4, CDC37, P62, and LC3. The housekeeping protein GAPDH was used as loading control.

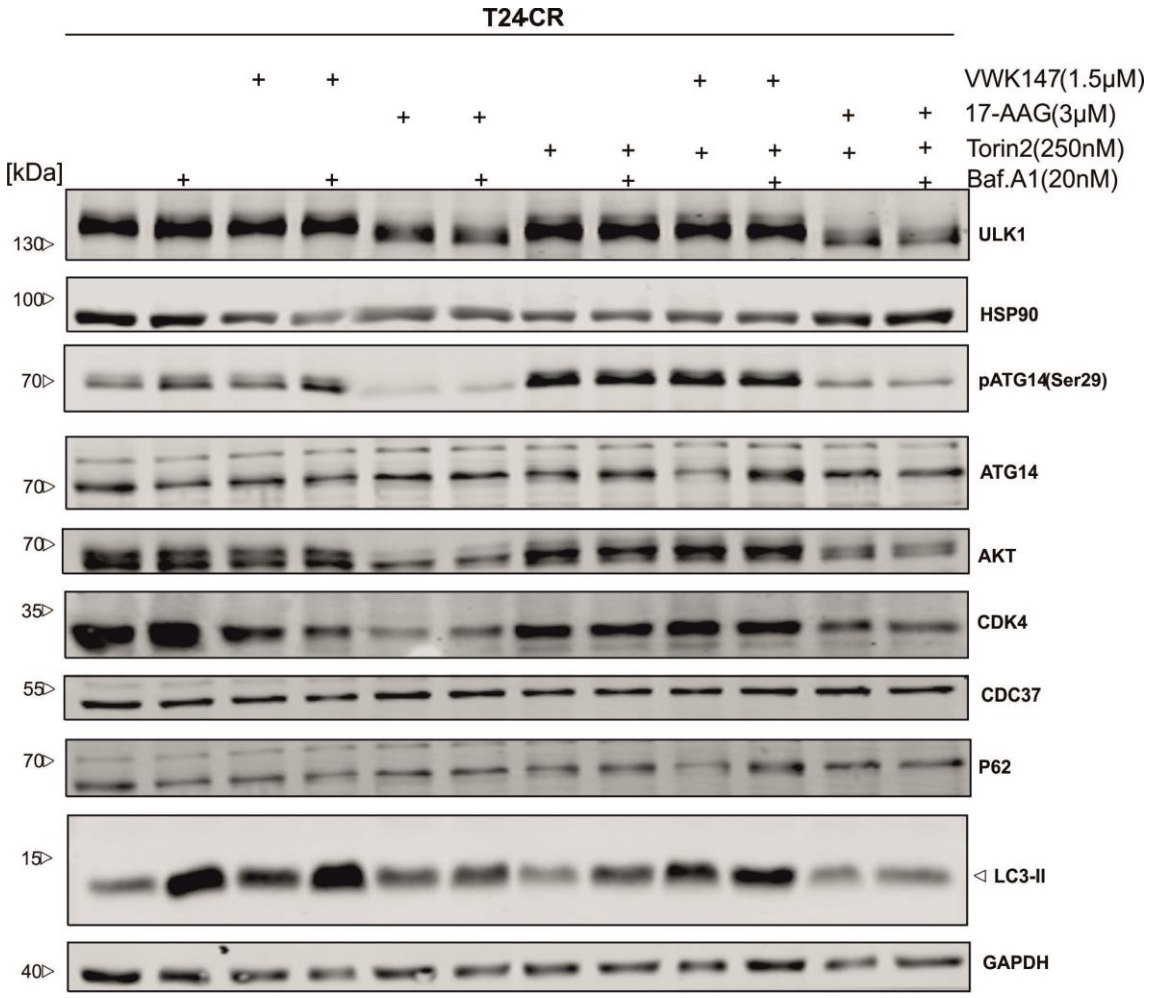

Figure 6.2.4: Immunoblotting results of Hsp90 clients and autophagy markers in T24-CR cells. T24-CR cells were treated with VWK147 (1.5 μM), 17-AAG (3 μM), Torin2 (250 nM), and Baf.A1 (20 nM) separately or in combination for 24 hours. After incubation, cells were collected by scraping and lysed. 25 μg of total protein were loaded on the SDS-PAGE gels and analyzed by immunoblotting. Samples were analyzed for ULK1, Hsp90, pATG14 ser29, ATG14, AKT, CDK4, CDC37, P62, and LC3. The housekeeping protein GAPDH was used as loading control.

7. Acknowledgements

I would like to take this opportunity to thank everyone who supported me throughout the years of my MD.

First of all, I would like to thank my supervisor Prof. Dr. Björn Stork, who gave me absolute freedom to perform the project I was interested in and highly skilled guidance throughout over the years.

I would like to thank my second supervisor Prof. Dr. Günter Niegisch for his support for my MD study and evaluating my dissertation.

Special thanks to Dr. Niklas Berleth for being my “executive” supervisor, who literally taught me everything in the lab and gave me all these brilliant protocols.

Thanks to Dr. Margaretha Skowron for providing the bladder cancer cells.

Thanks to Prof. Dr. Thomas Kurz for providing the VWK147.

Thank all the members of our lab who make my life in Germany so much more interesting: Dr. David Schlütermann; Dr. Jana Deitersen; Dr. Fabian Stuhldreier; Dr. Maria Jose Mendiburo; Dr. Christoph Peter; Jan Cox; Lena Berning; Annabelle Friedrich; Seda Akguen; Lea Esser; Dr. Gudrun Totzke.

At last, I would like to thank my cozy family: my parents, my wife and my little tough man for all your unconditional support and love. I will never make it without you all!